Received November 30, 2020, accepted December 27, 2020, date of publication January 6, 2021, date of current version January 19, 2021.

Digital Object Identifier 10.1109/ACCESS.2021.3049571

A Novel Cooperative Control System of Multi-Missile Formation Under Uncontrollable Speed

ZHENLIN ZHANG, KE ZHANG, AND ZHIGUO HAN
School of Astronautics, Northwestern Polytechnical University, Xi'an 710072, China
Corresponding author: Zhiguo Han (zghan2017@nwpu.edu.cn)

This work was supported by the Aviation Science Fund Project under Grant 20180153002.

ABSTRACT This article investigates a novel cooperative control system based on the sliding mode variable structure control theory for multi-missile formation flight. It is desired in practice to form and maintain the formation under the premise of uncontrollable missile speed. First, under the inertial coordinate system, we obtain the model of the formation control problem using the relative position of the leader to the follower. Then, we perform acceleration conversion and combine it to this model, getting the form of the formation problem model in the ballistic coordinate system. The finished model is useful for researchers to design the formation controller on this basis. Besides, the sliding mode variable structure control theory is used to design the formation controller for the system not considering disturbances and considering disturbances. Then we use the Lyapunov stability theory to analyze the stability of the formation control system. Finally, we compare our method with another method which requires controllable speed. According to numerical simulations, the method proposed in this article can achieve similar relative position errors under the condition of uncontrollable speed. And the robustness, versatility and formation adaptability of the method we propose are confirmed by simulation results.

INDEX TERMS Multi-missile formation, uncontrollable speed, sliding mode variable structure control, a leader-follower strategy.

NOMENCLATURE

X_l, Y_l, Z_l	Coordinate value of the leader in the inertial coordinate system
X_{fi}, Y_{fi}, Z_{fi}	Coordinate value of the *ith* follower in the inertial coordinate system
$\boldsymbol{L}(\psi_{Vl}, \theta_l)$	Transformation matrix of the leader from the inertial coordinate system to the ballistic coordinate system
$\boldsymbol{L}(\psi_{Vfi}, \theta_{fi})$	Transformation matrix of the *ith* follower from the inertial coordinate system to the ballistic coordinate system
$x_{iR}^*, y_{iR}^*, z_{iR}^*$	Expected position difference of the leader and the *ith* follower in the relative position coordinate system
x_i^*, y_i^*, z_i^*	Expected position difference of the leader and the *ith* follower in the inertial coordinate system
$V_{fi}^c, \theta_{fi}^c, \psi_{Vfi}^c$	Command of the velocity, the ballistic inclination angle, and the ballistic declination angle of the *ith* follower
$V_{fi}, \theta_{fi}, \psi_{Vfi}$	Velocity, ballistic inclination angle, and ballistic declination angle of the *ith* follower
θ_l, ψ_{Vl}	Ballistic inclination angle and ballistic declination angle of the leader
a_{nyl}, a_{nzl}	Acceleration of the leader's pitch and yaw channel
a_{nyfi}, a_{nzfi}	Acceleration of the *ith* follower's pitch and yaw channel
a_{xl}, a_{yl}, a_{zl}	Acceleration of the leader in the x, y and z axis of the inertial coordinate system
$a_{xfi}, a_{yfi}, a_{zfi}$	Acceleration of the *ith* follower in the x, y and z axis of the inertial coordinate system
$\boldsymbol{F}(t), \hat{\boldsymbol{F}}(t)$	Disturbance and its observational value

The associate editor coordinating the review of this manuscript and approving it for publication was Haibin Sun.

I. INTRODUCTION

A. BACKGROUND AND MOTIVATIONS

In recent years, with the development of missile defense systems in many countries, the ability of a single missile to penetrate and attack has been threatened. It is incapable of meeting the requirements put forward nowadays. During the combat, multiple missiles can form a formation system through information interaction, and jointly complete combat tasks such as searching, penetration, and saturation attack, etc. A formation system can greatly enhance the strike capability and the probability of destroying the target, and improve the penetration capability of the missile. So it is of great practical significance to study multi-missile formation.

There is a problem with the missile formation controller. In the mid-guidance stage, thrust of air-to-air missiles can not satisfy the control of speed in real time, so the speed of the missiles is uncontrollable [1]. Moreover, controlling speed may increase energy consumption. Therefore, we need to find a method of designing the multi-missile formation control system without controlling speed.

B. LITERATURE REVIEW

At present, the design of formation controllers mostly focuses on agents that has controllable speed in real time. The reason is that for these agents, it is easy to design the formation controller and apply it to reality.

Based on the algebraic graph theory, Han *et al.* designed a distributed formation tracking control algorithm through the fast terminal sliding mode control (FTSMC) scheme [2]. Huang *et al.* [3] adopted a disturbance state observer and then used the sliding mode control method to design a position and attitude tracking control law and studied the collision avoidance problem. And [4] considered the noise of wind and measurement in reality and proposed a control strategy based on the virtual structure. This method used the general topology of coupled agents to ensure the stability of multi-agents under the communication delay. Aiming at the limited time formation control problem of quadrotor UAVs, Du *et al.* designed a position and attitude controller including a limited period of time based on the reverse stepping method [5]. Amir *et al.* proposed a two-stage energy optimal reconstruction strategy, which moves agents to a special formation during the idle time between the issuance of current task and the next formation change command [6]. The method of [7] is the same as that in [6], except that the control of energy is replaced by the control of the formation change time. Aiming at the four-rotor UAV formation control problem, Zhao adopted a hierarchical method which consists of an upper model predictive controller (MPC) and a bottom robust feedback linearization controller [8]. Xu and Zen [9] used a multivariable model reference adaptive control (MRAC) method to design the control law in view of the uncertainty of the leader's parameters in formation control. Zhen *et al.* [10] considered the leader's dynamic uncertainty and unknown external disturbances, and designed the MRAC controller aiming at the UAV formation. For the problem of multi-agent collisions, [11] used the matrix transformation and the linear quadratic regulator theory to propose an optimal distributed formation control method. Although most of the formation control methods of other types of agents cannot be directly applied to the missiles, it can provide with design ideas.

There are relatively fewer references on the design of formation controllers for missiles. Many scholars used an autopilot to design the formation controller. Wang *et al.* considered multiple constraints such as the initial position, the end position and collision avoidance, and designed an optimal trajectory based on the Gaussian pseudo-spectrum method [12]. Wei *et al.* [13]–[15] all used an autopilot for formation controller design. Wei *et al.* [13] used an adaptive control method for formation controller design but [14], [15] used the optimal control theory for the formation controller design. Aiming at the problem of missile formation reconstruction, Ma *et al.* designed an optimal control method for missile formation reconstruction based on the Pseudo-spectral method [16]. Yu *et al.* proposed a time-varying formation tracking and control strategy using a leader-based guidance strategy [17]. Ma and Ji [18] and Wei *et al.* [19] both adopted the Leader-Follower formation mode and use the missile's autopilot to design the formation controller based on linear feedback and the optimal control theory. Peng *et al.* [20] designed a multi-missile formation flight control method based on the Leader-Follower method. It used the relative position between the leader and the follower to design a formation controller based on error feedback.

Some scholars did not use the autopilot to design the formation controller. Wang *et al.* studied the design problem of a multi-missile formation controller with aerodynamics in three-dimensional space. This method mainly solves the formation turning problem of large maneuverable aircraft [21]. Gao *et al.* designed a formation holding controller based on the stability of the follower to control the speed and height of the follower [22]. Zhang linearized the missile's nonlinear motion model through the differential geometry theory, and based on this, a formation controller was designed using the Leader-Follower missile guidance strategy and the adaptive sliding mode control theory [23]. Wang *et al.* regarded the relative velocity between the leader and the follower and the acceleration of the leader as estimable bounded uncertainties, and based on this designed a robust formation controller [24]. Zhang *et al.* [25] designed the formation controller by using the Leader-Follower strategy and the optimal control theory of affine nonlinear systems. Aiming at the formation tracking, external disturbances, and model uncertainties in the missile formation system, Zhou *et al.* proposed a robust adaptive formation based on a directional communication topology [26]. However, the above methods all have to control the speed of the missile, which does not meet the prerequisite that in reality, the missile speed is usually uncontrollable.

Many scholars have conducted in-depth research on sliding mode control. Mobayen *et al.* proposed a novel recursive singularity free FTSM (Fast Terminal Sliding Mode) strategy for finite-time tracking control of nonholonomic systems [27].

This method solved the singularity of the fractional power of the traditional sliding mode near the origin. Mobayen [28] proposed the control of a class of underactuated systems which are featured as in cascaded form with external disturbances. This method is derived from the first-order system differential equation and can deal with the disturbance and uncertainty of the system. Utkin studied sliding mode control of nonlinear systems with regular forms, which laid a foundation for the development of the sliding mode control theory [29]. For a class of nonlinear discrete random-switching systems, a comprehensive sliding mode control method based on the mean dwell time and the Lyapunov function method is proposed in [30]. Mobayen and M [31] proposed a new finite time robust tracking and model tracking control method based on a composite nonlinear feedback scheme for nonlinear time-delay uncertain chaotic systems.

Many scholars combined the disturbance observer with sliding mode control to solve the problem. Dong *et al.* [32] combined a nonlinear disturbance observer with the non-singular Terminal Sliding Mode Control (NTSMC). This method can restrain buffeting effectively and converge the system in the finite time. You *et al.* [33] proposed a control system combining a Uniform Robust Disturbance Observer (UREDO) with a non-singular terminal sliding mode controller. This scheme can track guidance commands within a certain time under model uncertainty and external disturbance in the system, and does not need the derivative of states and special initial conditions. So it is valuable in engineering applications. Meng Y proposed an Improved Sliding Mode Disturbance Observer (ISMDO). In this method, the terminal sliding mode control law is combined with an external anti-saturation system to compensate the saturation of the sliding mode surface, so that the controller can track the command smoothly. This method does not need to know the boundary of disturbances and faults, and has fewer undetermined parameters and better real-time performance [34]. Mobayen and Tchier [35] investigated a novel nonsingular fast terminal sliding-mode control method for the stabilization of the uncertain time-varying and nonlinear third-order systems. This method can overcome the singularity problem of the fast terminal sliding-mode control technique. No knowledge of the upper bound is required, thus eliminating the chattering problem.

C. CONTRIBUTIONS

Through the previous formation control research, all the formation controllers are designed under the condition that the velocity is controllable. But generally speaking, air-to-air missiles in the mid-guidance stage can not control the speed in real time during the mid-guidance stage. Moreover, controlling speed increases energy consumption. In recent years, this issue has not attracted enough attention, which is still open in the literature.

To solve the problem of uncontrollable speed, improve the anti-interference performance of the existing methods, and reduce the complexity of the model, we propose a formation control system with uncontrollable speed. Below we show the comparison of an existing method and the method proposed in this article. The structure of the controller of the leader is shown in Fig. 1. The formation control system of the method in [20] is shown in Fig. 2 and our control system is shown in Fig. 3.

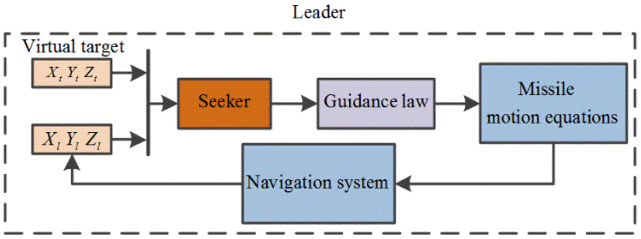

FIGURE 1. Formation controller of the leader.

Compared with the existing methods, the proposed method has some advantage as follows:

(1) The formation control system proposed in this article does not need to control the speed.
(2) We propose a general and less complex model of the formation control problem.
(3) The formation control system, based on the sliding mode variable structure control theory, is suitable for multiple formations and can overcome internal uncertainties and external disturbances.

The main contributions of this article are stated as follows:

(1) We start from the uncontrollable-speed condition for modelling, which is more in line with the requirements in reality.
(2) The formation control model is modelled in inertial system, which greatly reduces the complexity of the model.
(3) A linearized control model is obtained by applying coordinate and equation transformation, which provides a basis for the formation controller design.
(4) Sliding mode control is adopted to improve the robustness of the formation control system.

Under the premise that the speed of missiles is uncontrollable, firstly, we introduce the relative position of the leader and the follower, and define the state variables of the formation control problem in the inertial system, then design the model of the problem. To obtain the specific expression of the problem, the pitch and yaw acceleration of the missiles are transferred from the ballistic coordinate system to the inertial coordinate system. Secondly, aiming at the presence or absence of disturbances in the system, we design the formation controller using the sliding mode variable structure control theory. And the Lyapunov stability theory is used to prove the stability of the system. Finally, for the scenario that the leader attacks the virtual target (the predicted hit point) in the mid-guidance stage, we design simulation experiments using the formation formed by one leader and two followers. Comparing with an existing method which does not consider the speed change, we achieve the similar formation position

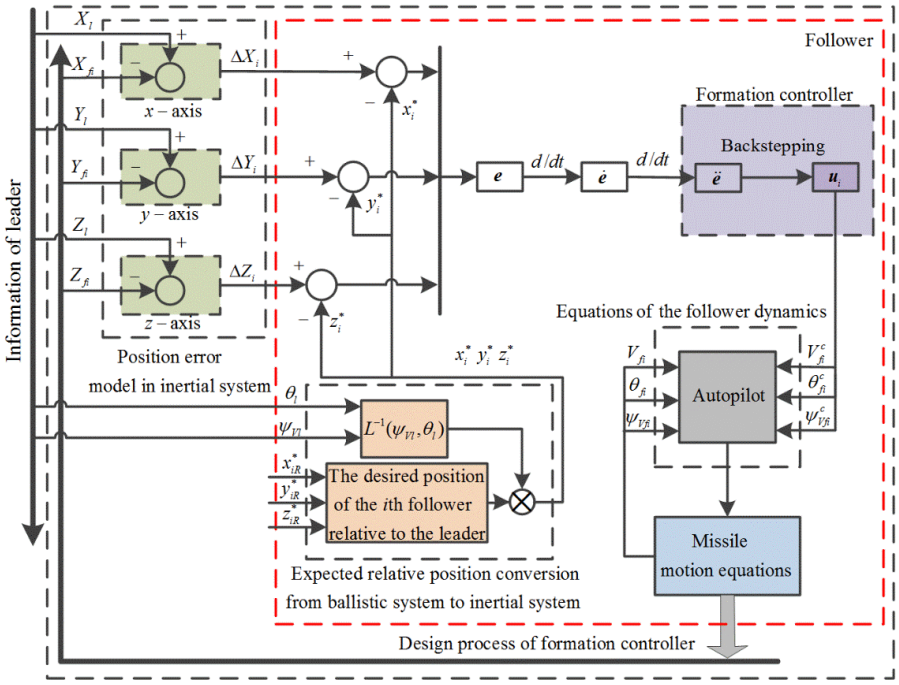

FIGURE 2. An existing formation control system [20].

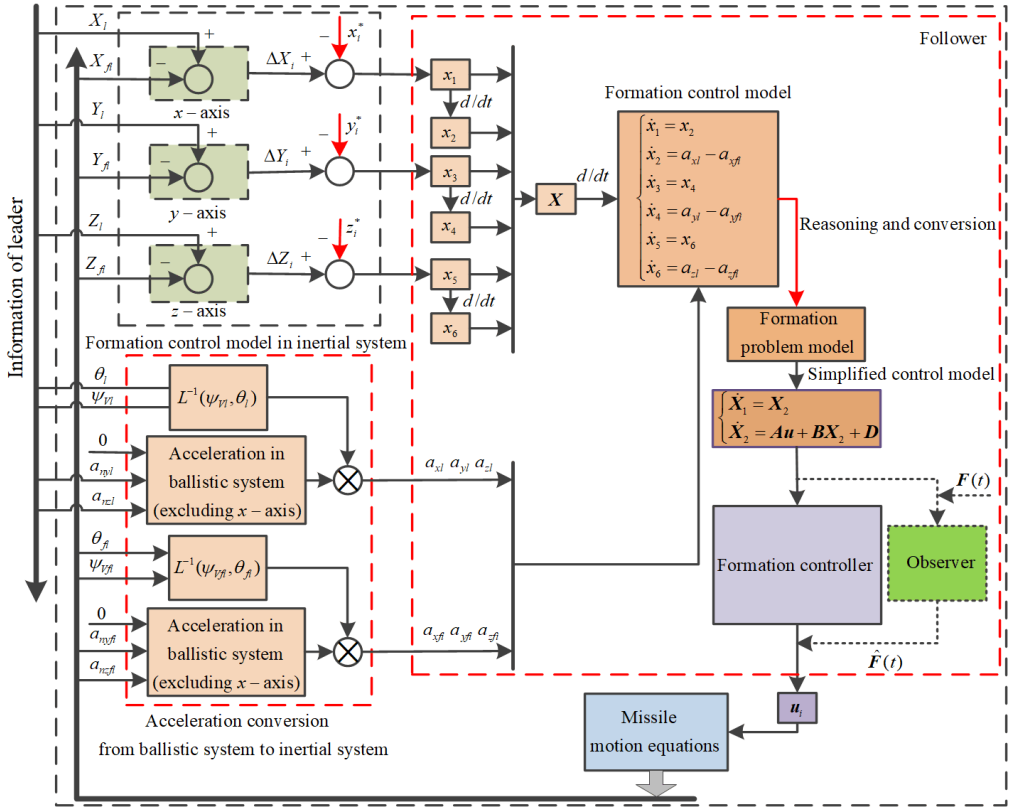

FIGURE 3. Formation control system proposed in this article.

error with that of the method. And we verify the method of designing the formation controller for both disturbed and non-disturbed conditions, and the effectiveness and feasibility of the method.

D. ARTICLE ORGANIZATION

The rest of this article is organized as follows. In Section 2, we design the model of the missile formation problem. In Section 3, aiming at the two situations of the presence

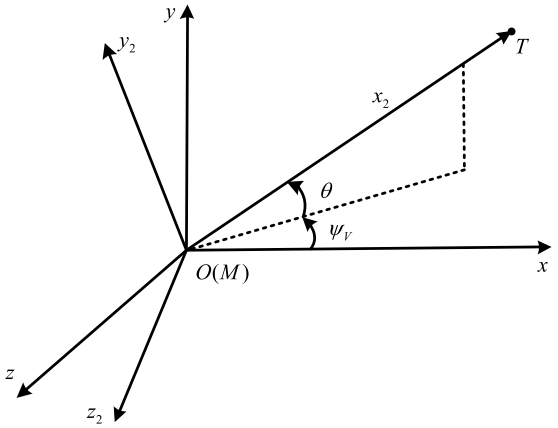

FIGURE 4. Three-dimensional interception geometry.

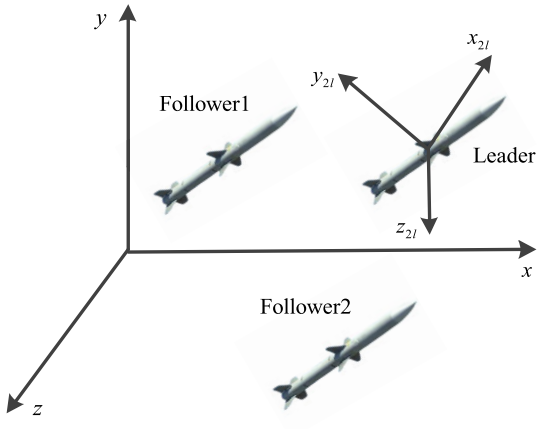

FIGURE 5. Leader's and follower's coordinate system.

or absence of disturbance in the system, we use the sliding mode variable structure control theory to design the formation controller for the leader and the follower. Then, the process of proving the stability of the controller is given. Simulation experiments are performed in Section 4 to demonstrate the superiority of the proposed method by comparing it with an existing method. Section 5 concludes this article. Section 6 includes the future recommendation.

II. DESIGN OF FORMATION CONTROL PROBLEM MODEL

In this section, we first give the basic knowledge of formation problem. Then we adopt the Leader-Follower strategy to design the model of formation control problem under uncontrollable speed.

A. BASIC KNOWLEDGE OF MISSILE FORMATION PROBLEM

A missile may have a small angle of view in the mid-guidance stage, resulting in that the target cannot be observed. To increase the probability that the missile finds the target in the mid-guidance stage, multiple missiles are used to form a formation and observe the target at the same time. Three-dimensional interception geometry is given in Fig. 4.

As shown in Fig. 4, $Oxyz$ denotes the inertial coordinate system; $Ox_2y_2z_2$ denotes the ballistic coordinate system; M and T denote the missile and target, respectively; θ and ψ_V denote the ballistic inclination angle and ballistic declination angle, respectively.

The transformation matrix of the missile from the inertial coordinate system to the ballistic coordinate system can be obtained by two rotations. First, we rotate the inertial coordinate system by angle ψ_V around the axis Oy, and then by angle θ around the axis Oz_2.

$$\begin{aligned} \boldsymbol{L}(\psi_V, \theta) &= \boldsymbol{L}(\theta)\boldsymbol{L}(\psi_V) \\ &= \begin{pmatrix} \cos\theta\cos\psi_V & \sin\theta & -\cos\theta\sin\psi_V \\ -\sin\theta\cos\psi_V & \cos\theta & \sin\theta\sin\psi_V \\ \sin\psi_V & 0 & \cos\psi_V \end{pmatrix} \end{aligned} \tag{1}$$

The kinematic equation set of the missile is:

$$\begin{cases} \dot{x} = V\cos\theta\cos\psi_V \\ \dot{y} = V\sin\theta \\ \dot{z} = -V\cos\theta\sin\psi_V \end{cases} \tag{2}$$

Before designing the formation model, we make the following assumptions:

(1) The missile can be regarded as a mass point and its speed is a constant;
(2) The acceleration direction of the missile is perpendicular to the velocity direction, which means acceleration only changes the direction of the speed, not the value of the speed;
(3) Usually, the response of dynamic characteristics in the missile is fast, so we ignore its dynamic characteristics. That is, $a_{ny} = a_{ny}^c$, $a_{nz} = a_{nz}^c$. a_{ny} and a_{nz} denote the missile's acceleration in the pitch and the yaw channel, respectively; a_{ny}^c and a_{nz}^c denote the command of acceleration in the pitch and the yaw channel, respectively.

B. FORMATION PROBLEM MODEL

In this section, we describe the difference between the actual and expected distance of the leader and the follower in the inertial coordinate system. Then the Leader-Follower guidance strategy is adopted to design the formation control model. After this, we propose the formation control model that does not need the controllable speed. Based on this model, it is convenient for readers to design the formation controller. The definition of the leader's and the follower's coordinate system is shown in Fig. 5. The transition of information between the leader and the follower is one-way, which means the follower can receive information from the leader but the leader cannot receive information from the follower. The leader attacks the virtual target under the designed guidance law. The relative positional relationship between the leader and the *ith* follower in the inertial coordinate system is shown in Fig. 6.

In Fig. 6, M_l and M_{fi} denote the leader and the *ith* follower, respectively; X_l, Y_l, Z_l denote the coordinate value of the

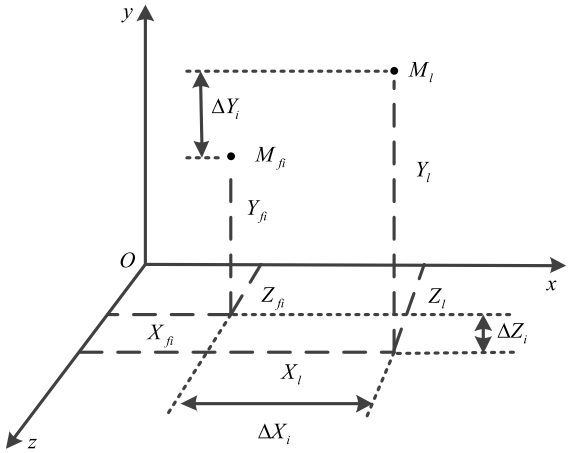

FIGURE 6. Relative position relationship between leader and follower.

leader in the x, y and z axis of the inertial coordinate system, respectively; X_{fi}, Y_{fi}, Z_{fi} denote the coordinate value of the leader and the *ith* follower in the x, y and z axis of the inertial coordinate system, respectively; and ΔX_i, ΔY_i and ΔZ_i denote the difference of the position of the leader and the *ith* follower in the x, y and z axis of the inertial coordinate system, respectively. The definition equation of ΔX_i, ΔY_i and ΔZ_i is given below:

$$\begin{cases} \Delta X_i = X_l - X_{fi} \\ \Delta Y_i = Y_l - Y_{fi} \\ \Delta Z_i = Z_l - Z_{fi} \end{cases} \tag{3}$$

Defining state variables: $x_1 = X_l - X_{fi} - x_i^*$, $x_2 = \dot{X}_l - \dot{X}_{fi}$, $x_3 = Y_l - Y_{fi} - y_i^*$, $x_4 = \dot{Y}_l - \dot{Y}_{fi}$, $x_5 = Z_l - Z_{fi} - z_i^*$, $x_6 = \dot{Z}_l - \dot{Z}_{fi}$, where x_i^*, y_i^* and z_i^* denote the expected position difference between the leader and the *ith* follower in the x, y and z axis of the inertial coordinate system, respectively. Therefore, the model of the formation control problem in three-dimensional space can be expressed as below:

$$\begin{cases} \dot{x}_1 = x_2 \\ \dot{x}_2 = \ddot{X}_l - \ddot{X}_{fi} = a_{xl} - a_{xfi} \\ \dot{x}_3 = x_4 \\ \dot{x}_4 = \ddot{Y}_l - \ddot{Y}_{fi} = a_{yl} - a_{yfi} \\ \dot{x}_5 = x_6 \\ \dot{x}_6 = \ddot{Z}_l - \ddot{Z}_{fi} = a_{zl} - a_{zfi} \end{cases} \tag{4}$$

where a_{xl}, a_{yl} and a_{zl} denote the acceleration of the leader, respectively; a_{xfi}, a_{yfi} and a_{zfi} denote the acceleration of the *ith* follower, respectively. The x, y and z axis here is in the inertial coordinate system.

We define that in the ballistic coordinate system, the acceleration of the leader's pitch and yaw channel is a_{nyl} and a_{nzl}, and the acceleration of the *ith* follower's pitch and yaw channel is a_{nyfi} and a_{nzfi}. And according to the transformation matrix from the inertial coordinate system to the ballistic coordinate system, the inverse transformation matrix can be obtained:

$$\boldsymbol{L}^{-1}(\psi_V, \theta) = \begin{pmatrix} \cos\theta\cos\psi_V & -\sin\theta\cos\psi_V & \sin\psi_V \\ \sin\theta & \cos\theta & 0 \\ -\cos\theta\sin\psi_V & \sin\theta\sin\psi_V & \cos\psi_V \end{pmatrix} \tag{5}$$

Then we convert the acceleration of the leader and the follower from the ballistic coordinate system to the inertial coordinate system.

$$\begin{pmatrix} a_{xl} \\ a_{yl} \\ a_{zl} \end{pmatrix} = \boldsymbol{L}^{-1}(\psi_{Vl}, \theta_l) \begin{pmatrix} 0 \\ a_{nyl} \\ a_{nzl} \end{pmatrix} \tag{6}$$

$$\begin{pmatrix} a_{xfi} \\ a_{yfi} \\ a_{zfi} \end{pmatrix} = \boldsymbol{L}^{-1}(\psi_{Vfi}, \theta_{fi}) \begin{pmatrix} 0 \\ a_{nyfi} \\ a_{nzfi} \end{pmatrix} \tag{7}$$

Substituting (5) into (6) and (7), we can get the specific expressions for the acceleration of the leader and the follower in the inertial coordinate system.

$$\begin{pmatrix} a_{xl} \\ a_{yl} \\ a_{zl} \end{pmatrix} = \begin{pmatrix} -\sin\theta_l\cos\psi_{Vl}a_{nyl} + \sin\psi_{Vl}a_{nzl} \\ \cos\theta_l a_{nyl} \\ \sin\theta_l\sin\psi_{Vl}a_{nyl} + \cos\psi_{Vl}a_{nzl} \end{pmatrix} \tag{8}$$

$$\begin{pmatrix} a_{xfi} \\ a_{yfi} \\ a_{zfi} \end{pmatrix} = \begin{pmatrix} -\sin\theta_{fi}\cos\psi_{Vfi}a_{nyfi} + \sin\psi_{Vfi}a_{nzfi} \\ \cos\theta_{fi}a_{nyfi} \\ \sin\theta_{fi}\sin\psi_{Vfi}a_{nyfi} + \cos\psi_{Vfi}a_{nzfi} \end{pmatrix} \tag{9}$$

Substituting (8) and (9) into (4), the formation control problem model can be obtained:

$$\begin{cases} \dot{x}_1 = x_2 \\ \dot{x}_2 = -\sin\theta_l\cos\psi_{Vl}a_{nyl} + \sin\psi_{Vl}a_{nzl} \\ \qquad + \sin\theta_{fi}\cos\psi_{Vfi}a_{nyfi} - \sin\psi_{Vfi}a_{nzfi} \\ \dot{x}_3 = x_4 \\ \dot{x}_4 = \cos\theta_l a_{nyl} - \cos\theta_{fi}a_{nyfi} \\ \dot{x}_5 = x_6 \\ \dot{x}_6 = \sin\theta_l\sin\psi_{Vl}a_{nyl} + \cos\psi_{Vl}a_{nzl} \\ \qquad - \sin\theta_{fi}\sin\psi_{Vfi}a_{nyfi} - \cos\psi_{Vfi}a_{nzfi} \end{cases} \tag{10}$$

Observing (10), after reasoning and conversion, the specific expression of the model can be obtained:

$$\begin{cases} \dot{x}_1 = x_2 \\ \dot{x}_2 = \sin\theta_{fi}\cos\psi_{Vfi}a_{nyfi} - \sin\psi_{Vfi}a_{nzfi} \\ \qquad - \dfrac{V_{fi}}{V_l}\tan\theta_l a_{nyl}\cos\theta_{fi}\cos\psi_{Vfi} \\ \qquad + \sin\psi_{Vl}a_{nzl} - \dfrac{\sin\theta_l a_{nyl}}{V_l\cos\theta_l}x_2 \\ \dot{x}_3 = x_4 \\ \dot{x}_4 = -\cos\theta_{fi}a_{nyfi} + \dfrac{V_{fi}\sin\theta_{fi}\cos\theta_l a_{nyl}}{V_l\sin\theta_l} + \dfrac{\cos\theta_l a_{nyl}}{V_l\sin\theta_l}x_4 \\ \dot{x}_5 = x_6 \\ \dot{x}_6 = -\sin\theta_{fi}\sin\psi_{Vfi}a_{nyfi} - \cos\psi_{Vfi}a_{nzfi} \\ \qquad + \dfrac{V_{fi}}{V_l}\tan\theta_l\cos\theta_{fi}\sin\psi_{Vfi}a_{nyl} + \cos\psi_{Vl}a_{nzl} \\ \qquad - \dfrac{\tan\theta_l a_{nyl}}{V_l}x_6 \end{cases} \tag{11}$$

To make the design process of the controller in Section 3 easier, we simplify (11) as below:

$$
\begin{aligned}
&A_1 = \sin\theta_{fi}\cos\psi_{Vfi}, \quad A_2 = -\sin\psi_{Vfi}, \; A_3 = -\cos\theta_{fi},\\
&A_4 = -\sin\theta_{fi}\sin\psi_{Vfi}, \quad A_5 = -\cos\psi_{Vfi};\\
&B_1 = -\frac{\sin\theta_l a_{nyl}}{V_l\cos\theta_l}, \quad B_2 = \frac{\cos\theta_l a_{nyl}}{V_l\sin\theta_l}, \; B_3 = -\frac{\tan\theta_l a_{nyl}}{V_l};\\
&D_1 = -\frac{V_{fi}}{V_l}\tan\theta_l\cos\theta_{fi}\cos\psi_{Vfi}a_{nyl} + \sin\psi_{Vl}a_{nzl},\\
&D_2 = \frac{V_{fi}\sin\theta_{fi}\cos\theta_l a_{nyl}}{V_l\sin\theta_l},\\
&D_3 = \frac{V_{fi}}{V_l}\tan\theta_l\cos\theta_{fi}\sin\psi_{Vfi}a_{nyl} + \cos\psi_{Vl}a_{nzl},\\
&u_1 = a_{nyfi}, \quad u_2 = a_{nzfi}.
\end{aligned}
$$

Substituting the above simplification into (11), a simplified form of the formation control model can be obtained:

$$
\begin{cases}
\dot{x}_1 = x_2\\
\dot{x}_2 = A_1u_1 + A_2u_2 + B_1x_2 + D_1\\
\dot{x}_3 = x_4\\
\dot{x}_4 = A_3u_1 + B_2x_4 + D_2\\
\dot{x}_5 = x_6\\
\dot{x}_6 = A_4u_1 + A_5u_2 + B_3x_6 + D_3
\end{cases} \tag{12}
$$

Observing the above equation, we can simplify it one step further. We define

$$
\boldsymbol{A} = \begin{pmatrix} A_1 & A_2\\ A_3 & 0\\ A_4 & A_5 \end{pmatrix}, \quad \boldsymbol{B} = \begin{pmatrix} B_1 & 0 & 0\\ 0 & B_2 & 0\\ 0 & 0 & B_3 \end{pmatrix}, \quad \boldsymbol{D} = \begin{pmatrix} D_1\\ D_2\\ D_3 \end{pmatrix},
$$

$$
\boldsymbol{u} = \begin{pmatrix} u_1\\ u_2 \end{pmatrix}, \quad \boldsymbol{X}_1 = \begin{pmatrix} x_1\\ x_3\\ x_5 \end{pmatrix}, \; \boldsymbol{X}_2 = \begin{pmatrix} x_2\\ x_4\\ x_6 \end{pmatrix}.
$$

Substituting the above matrices into (12), the further simplified model of the formation control problem can be obtained:

$$
\begin{cases}
\dot{\boldsymbol{X}}_1 = \boldsymbol{X}_2\\
\dot{\boldsymbol{X}}_2 = \boldsymbol{A}\boldsymbol{u} + \boldsymbol{B}\boldsymbol{X}_2 + \boldsymbol{D}
\end{cases} \tag{13}
$$

III. DESIGN OF MULTI-MISSILE FORMATION CONTROLLER

In this article, we adopt the Leader-Follower formation mode to design the formation controller. Considering the two cases of presence or absence of disturbance, we use the sliding mode variable structure control theory to design the guidance law of the leader and the follower respectively. Finally, the Lyapunov stability theory is used to give stability proof.

A. DESIGN THE CONTROLLER OF THE LEADER

The sliding mode variable structure theory in [36] is used to design the controller of the leader. The specific form is as follows:

$$
a_{nyl} = m\,|\dot{r}_l|\,\dot{q}_{\varepsilon l} + \frac{|\dot{r}_l|}{r_l}n\frac{\dot{q}_{\varepsilon l}}{|\dot{q}_{\varepsilon l}| + \delta_1} \tag{14}
$$

$$
a_{nzl} = -m\,|\dot{r}_{1l}|\,\dot{q}_{\beta l} - \frac{|\dot{r}_{1l}|}{r_l}n\frac{\dot{q}_{\beta l}}{|\dot{q}_{\beta l}| + \delta_2} \tag{15}
$$

where, r_l and $\dot{r}_l$ denote the distance between the leader and the virtual target and its change rate, respectively; $\dot{q}_{\varepsilon l}$ and $\dot{q}_{\beta l}$ denote the change rate of the inclination and that of the declination of the line of sight, respectively. $r_{1l} = r\cos q_{\varepsilon l}$, $m > 0, n > 0, 0 < \delta_1 < 0.1, 0 < \delta_2 < 0.1$.

B. DESIGN THE CONTROLLER OF THE FOLLOWER (IGNORING DISTURBANCE)

In this section, we adopt the sliding mode variable structure control theory to design the controller for the model without disturbance. Then we use the Lyapunov stability theory to analyze the stability of the controller.

1) DESIGN OF THE CONTROLLER

For the formation controller model without disturbances derived in the previous section, we adopt the sliding mode variable structure control theory to design the controller in this section.

Observing the system model shown in (13), we select a linear sliding mode to design the controller for the system. The specific form of the linear sliding mode surface is [37]:

$$
\boldsymbol{s}_i = \boldsymbol{k}_{1i}\boldsymbol{X}_1 + \boldsymbol{k}_{2i}\boldsymbol{X}_2 + \boldsymbol{k}_{3i}\mathrm{sig}^{\alpha_i}(\boldsymbol{X}_1) \tag{16}
$$

where $\boldsymbol{s}_i = \begin{bmatrix} s_{1i} & s_{2i} & s_{3i} \end{bmatrix}^T$, $\mathrm{sig}^{\alpha_i}(\boldsymbol{X}_1) = \|\boldsymbol{X}_1\|^{\alpha_i}\,\mathrm{sign}(\boldsymbol{X}_1)$, $\boldsymbol{k}_{1i} = \mathrm{diag}(k_{11i}, k_{12i}, k_{13i}), k_{1ji} > 0 (j = 1, 2, 3), \boldsymbol{k}_{2i} = \mathrm{diag}(k_{21i}, k_{22i}, k_{23i}), k_{2ji} > 0 (j = 1, 2, 3), \boldsymbol{k}_{3i} = \mathrm{diag}(k_{31i}, k_{32i}, k_{33i}), k_{3ji} > 0 (j = 1, 2, 3), 1 < \alpha_i < 2$.

Then the derivative of the sliding mode surface can be obtained:

$$
\begin{aligned}
\dot{\boldsymbol{s}}_i &= \boldsymbol{k}_{1i}\dot{\boldsymbol{X}}_1 + \boldsymbol{k}_{2i}\dot{\boldsymbol{X}}_2 + \boldsymbol{k}_{3i}\alpha_i\,\|\boldsymbol{X}_1\|^{\alpha_i - 1}\dot{\boldsymbol{X}}_1\\
&= \boldsymbol{k}_{1i}\boldsymbol{X}_2 + \boldsymbol{k}_{2i}(\boldsymbol{A}\boldsymbol{u} + \boldsymbol{B}\boldsymbol{X}_2 + \boldsymbol{D}) + \boldsymbol{k}_{3i}\alpha_i\,\|\boldsymbol{X}_1\|^{\alpha_i - 1}\boldsymbol{X}_2
\end{aligned} \tag{17}
$$

Choosing the exponential approach as:

$$
\dot{\boldsymbol{s}}_i = -\boldsymbol{\varepsilon}_i\mathrm{sign}(\boldsymbol{s}_i) - \boldsymbol{k}_{4i}\boldsymbol{s}_i \tag{18}
$$

where $\boldsymbol{\varepsilon}_i = \mathrm{diag}(\varepsilon_{1i}, \varepsilon_{2i}, \varepsilon_{3i})$, $\boldsymbol{k}_{4i} = \mathrm{diag}(k_{41i}, k_{42i}, k_{43i})$, $\varepsilon_j, k_{4ji} > 0 (i = 1, 2, 3)$.

Substituting (18) into (17), we obtain:

$$
\begin{aligned}
\boldsymbol{k}_{2i}\boldsymbol{A}\boldsymbol{u} = &-\boldsymbol{\varepsilon}_i\mathrm{sign}(\boldsymbol{s}_i) - \boldsymbol{k}_{4i}\boldsymbol{s}_i - \boldsymbol{k}_{2i}\boldsymbol{D}\\
&-(\boldsymbol{k}_{1i} + \boldsymbol{k}_{3i}\alpha_i\,\|\boldsymbol{X}_1\|^{\alpha_i - 1} + \boldsymbol{k}_{2i}\boldsymbol{B})\boldsymbol{X}_2
\end{aligned} \tag{19}
$$

As it can be seen from (19), it is necessary to inverse the matrix $\boldsymbol{A}$, but $\boldsymbol{A}$ is not a square matrix. By using its pseudo-inverse form $\boldsymbol{A}^T(\boldsymbol{A}\boldsymbol{A}^T)^{-1}$ instead, we can further obtain the expression of the acceleration:

$$
\begin{aligned}
\boldsymbol{u}_i = \boldsymbol{A}^T(\boldsymbol{A}\boldsymbol{A}^T)^{-1}\boldsymbol{k}_{2i}^{-1}(&-\boldsymbol{\varepsilon}_i\mathrm{sign}(\boldsymbol{s}_i) - \boldsymbol{k}_{4i}\boldsymbol{s}_i\\
&-\boldsymbol{k}_{2i}\boldsymbol{D} - (\boldsymbol{k}_{1i} + \boldsymbol{k}_{3i}\alpha_i\,\|\boldsymbol{X}_1\|^{\alpha_i - 1} + \boldsymbol{k}_{2i}\boldsymbol{B})\boldsymbol{X}_2)
\end{aligned} \tag{20}
$$

2) STABILITY ANALYSIS

Theorem 1: For the deduced formation model in (13) under the condition of uncontrollable speed, we use the sliding mode surface in (16) and the reaching law in (18) to get the controller in (20) that can achieve and maintain formation.

Proof: Choosing a Lyapunov function $V_1 = \frac{1}{2}\boldsymbol{s}_i^T\boldsymbol{s}_i$. Obviously, V_1 is positive definite and continuous.

Differentiating V_1, we can get $\dot{V}_1$ as

$$\begin{aligned}\dot{V}_1 &= \boldsymbol{s}_i^T\dot{\boldsymbol{s}}_i \\ &= \boldsymbol{s}_i^T(\boldsymbol{k}_{1i}\boldsymbol{X}_2 + \boldsymbol{k}_{2i}(\boldsymbol{A}\boldsymbol{u} + \boldsymbol{B}\boldsymbol{X}_2 + \boldsymbol{D}) \\ &\quad + \boldsymbol{k}_{3i}\alpha_i \|\boldsymbol{X}_1\|^{\alpha_i-1}\boldsymbol{X}_2) \\ &= \boldsymbol{s}_i^T\boldsymbol{k}_{1i}\boldsymbol{X}_2 + \boldsymbol{s}_i^T\boldsymbol{k}_{2i}\boldsymbol{A}\boldsymbol{u} + \boldsymbol{s}_i^T\boldsymbol{k}_{2i}\boldsymbol{B}\boldsymbol{X}_2 \\ &\quad + \boldsymbol{s}_i^T\boldsymbol{k}_{2i}\boldsymbol{D} + \boldsymbol{s}_i^T\boldsymbol{k}_{3i}\alpha_i\|\boldsymbol{X}_1\|^{\alpha_i-1}\boldsymbol{X}_2 \\ &= \boldsymbol{s}_i^T\boldsymbol{k}_{1i}\boldsymbol{X}_2 + \boldsymbol{s}_i^T\boldsymbol{k}_{2i}\boldsymbol{B}\boldsymbol{X}_2 + \boldsymbol{s}_i^T\boldsymbol{k}_{2i}\boldsymbol{D} \\ &\quad + \boldsymbol{s}_i^T\boldsymbol{k}_{3i}\alpha_i\|\boldsymbol{X}_1\|^{\alpha_i-1}\boldsymbol{X}_2 + \boldsymbol{s}_i^T(-\boldsymbol{\varepsilon}_i\mathrm{sign}(\boldsymbol{s}_i) \\ &\quad - \boldsymbol{k}_{4i}\boldsymbol{s}_i - \boldsymbol{k}_{2i}\boldsymbol{D} - (\boldsymbol{k}_{1i} + \boldsymbol{k}_{3i}\alpha_i\|\boldsymbol{X}_1\|^{\alpha_i-1} + \boldsymbol{k}_{2i}\boldsymbol{B})\boldsymbol{X}_2) \\ &= \boldsymbol{s}_i^T\boldsymbol{k}_{1i}\boldsymbol{X}_2 + \boldsymbol{s}_i^T\boldsymbol{k}_{2i}\boldsymbol{B}\boldsymbol{X}_2 + \boldsymbol{s}_i^T\boldsymbol{k}_{2i}\boldsymbol{D} \\ &\quad + \boldsymbol{s}_i^T\boldsymbol{k}_{3i}\alpha_i\|\boldsymbol{X}_1\|^{\alpha_i-1}\boldsymbol{X}_2 - \boldsymbol{s}_i^T\boldsymbol{\varepsilon}_i\mathrm{sign}(\boldsymbol{s}_i) \\ &\quad - \boldsymbol{s}_i^T\boldsymbol{k}_{4i}\boldsymbol{s}_i - \boldsymbol{s}_i^T\boldsymbol{k}_{2i}\boldsymbol{D} - \boldsymbol{s}_i^T(\boldsymbol{k}_{1i} + \boldsymbol{k}_{3i}\alpha_i\|\boldsymbol{X}_1\|^{\alpha_i-1} + \boldsymbol{k}_{2i}\boldsymbol{B})\boldsymbol{X}_2 \\ &= -\boldsymbol{s}_i^T\boldsymbol{\varepsilon}_i\mathrm{sign}(\boldsymbol{s}_i) - \boldsymbol{s}_i^T\boldsymbol{k}_{4i}\boldsymbol{s}_i \end{aligned} \tag{21}$$

Observing (21), due to

$$\mathrm{sign}(s)s = \begin{cases} s, & s > 0 \\ -s, & s < 0 \end{cases} \tag{22}$$

and since $\boldsymbol{\varepsilon}_i > 0$ and $\boldsymbol{k}_{4i} > 0$, we can get

$$\boldsymbol{s}_i^T\boldsymbol{\varepsilon}_i\mathrm{sign}(\boldsymbol{s}_i) \geq 0 \tag{23}$$

$$\boldsymbol{s}_i^T\boldsymbol{k}_{4i}\boldsymbol{s}_i \geq 0 \tag{24}$$

From (21), we can know that

$$\dot{V}_1 \leq -\boldsymbol{s}_i^T\boldsymbol{\varepsilon}_i\mathrm{sign}(\boldsymbol{s}_i) - \boldsymbol{s}_i^T\boldsymbol{k}_{4i}\boldsymbol{s}_i \tag{25}$$

If we let $\dot{V}_1 = 0$, we can derive $\boldsymbol{s}_i = 0$. According to (16), the expression of $\boldsymbol{s}_i$ is shown below.

$$\boldsymbol{s}_i = \boldsymbol{k}_{1i}\boldsymbol{X}_1 + \boldsymbol{k}_{2i}\boldsymbol{X}_2 + \boldsymbol{k}_{3i}\mathrm{sig}^{\alpha_i}(\boldsymbol{X}_1) \tag{26}$$

Assuming that $\boldsymbol{X}_1 = 0$ and substituting it into (26), $\boldsymbol{X}_2 = 0$ can be obtained. Therefore, $\dot{V}_1 = 0$ can only be obtained when $\boldsymbol{X}_1 = 0$ and $\boldsymbol{X}_2 = 0$. This result cannot be obtained at any other points. So according to the principle of invariance [38], it can be obtained that:

$$\dot{V}_1 < 0 \tag{27}$$

So $\dot{V}_1 < 0$, which means the system state can reach the sliding mode surface. According to the Lyapunov stability theory, the system is progressively stable. The sliding mode surface $\boldsymbol{s}_i$ designed in this article can converge to zero in the finite time. The system state at that time is

$$\boldsymbol{k}_{1i}\boldsymbol{X}_1 + \boldsymbol{k}_{2i}\boldsymbol{X}_2 + \boldsymbol{k}_{3i}\mathrm{sig}^{\alpha_i}(\boldsymbol{X}_1) = \boldsymbol{s}_i = \boldsymbol{0} \tag{28}$$

The state equation of the system can be written as

$$\boldsymbol{X}_2 = \boldsymbol{k}_{2i}^{-1}(-\boldsymbol{k}_{1i}\boldsymbol{X}_1 - \boldsymbol{k}_{3i}\mathrm{sig}^{\alpha_i}(\boldsymbol{X}_1)) \tag{29}$$

Selecting another Lyapunov function as

$$V_2 = \frac{1}{2}\boldsymbol{X}_1^T\boldsymbol{X}_1 \tag{30}$$

Then we differentiate (30) as

$$\dot{V}_2 = \boldsymbol{X}_1^T\dot{\boldsymbol{X}}_1 = \boldsymbol{X}_1^T\boldsymbol{X}_2 \tag{31}$$

Substituting (29) into (31), we can get

$$\begin{aligned}\dot{V}_2 &= \boldsymbol{X}_1^T\dot{\boldsymbol{X}}_1 = \boldsymbol{X}_1^T\boldsymbol{X}_2 \\ &= \boldsymbol{X}_1^T\boldsymbol{k}_{2i}^{-1}(-\boldsymbol{k}_{1i}\boldsymbol{X}_1 - \boldsymbol{k}_{3i}\mathrm{sig}^{\alpha_i}(\boldsymbol{X}_1)) \\ &= -\boldsymbol{k}_{2i}^{-1}\boldsymbol{k}_{1i}\boldsymbol{X}_1^T\boldsymbol{X}_1 - \boldsymbol{k}_{2i}^{-1}\boldsymbol{k}_{3i}\boldsymbol{X}_1^T\mathrm{sig}^{\alpha_i}(\boldsymbol{X}_1) \\ &= -\boldsymbol{k}_{2i}^{-1}\boldsymbol{k}_{1i}\boldsymbol{X}_1^T\boldsymbol{X}_1 - \boldsymbol{k}_{2i}^{-1}\boldsymbol{k}_{3i}\boldsymbol{X}_1^T\|\boldsymbol{X}_1\|^{\alpha_i}\mathrm{sign}(\boldsymbol{X}_1) \\ &= -\boldsymbol{k}_{2i}^{-1}\boldsymbol{k}_{1i}\|\boldsymbol{X}_1\| - \boldsymbol{k}_{2i}^{-1}\boldsymbol{k}_{3i}\|\boldsymbol{X}_1\|^{\alpha_i+1} \\ &\leq 0 \end{aligned} \tag{32}$$

From (32), according to the principle of invariance, we know that $\dot{V}_2 < 0$, so the system state can converge. According to the Lyapunov stability theory, the system is gradually stable, which means when $t \to \infty$, $\boldsymbol{X}_1 \to 0$.

$$\begin{cases} \lim\limits_{t\to\infty}\Delta X_i = x_i^* \\ \lim\limits_{t\to\infty}\Delta Y_i = y_i^* \\ \lim\limits_{t\to\infty}\Delta Z_i = z_i^* \end{cases} \tag{33}$$

According to (33), the position difference ΔX_i, ΔY_i and ΔZ_i can converge to the expected value in each axis, respectively.

Note that the formation control function shown in (20) has a sign function term. To reduce chattering, the sign function is replaced with a saturation function, and the controller can be rewritten as

$$\begin{aligned}\boldsymbol{u}_i = \boldsymbol{A}^T(\boldsymbol{A}\boldsymbol{A}^T)^{-1}\boldsymbol{k}_{2i}^{-1}(-\boldsymbol{\varepsilon}_i\mathrm{sat}(\boldsymbol{s}_i) - \boldsymbol{k}_{4i}\boldsymbol{s}_i \\ - \boldsymbol{k}_{2i}\boldsymbol{D} - (\boldsymbol{k}_{1i} + \boldsymbol{k}_{3i}\alpha_i\|\boldsymbol{X}_1\|^{\alpha_i-1} + \boldsymbol{k}_{2i}\boldsymbol{B})\boldsymbol{X}_2)\end{aligned} \tag{34}$$

The expression of the saturation function is

$$\mathrm{sat}(\boldsymbol{s}_i) = \begin{cases} \mathrm{sign}(\boldsymbol{s}_i) & \|\boldsymbol{s}_i\| > \sigma_i \\ \dfrac{\boldsymbol{s}_i}{\sigma_i} & \|\boldsymbol{s}_i\| \leq \sigma_i \end{cases} \tag{35}$$

where $\sigma_i > 0$, when $\|\boldsymbol{s}_i\| > \sigma_i$, $\mathrm{sat}(\boldsymbol{s}_i) = \mathrm{sign}(\boldsymbol{s}_i)$. Therefore, replacing the sign function with a saturation function not only has no impact on the convergence effect of the system, but also can improve the stability of the missile and make control performance better.

C. DESIGN THE CONTROLLER OF THE FOLLOWER (CONSIDERING DISTURBANCE)

In this section, through the similar process with Section B, we design the controller for the model with disturbance and analyze the stability.

1) DESIGN OF THE CONTROLLER

For the controller design in Section B, factors like disturbances and linearization errors are not considered. In this section we take them into consideration, and we can get the

formation control problem model with external disturbances and linearization errors:

$$\begin{cases} \dot{\boldsymbol{X}}_1 = \boldsymbol{X}_2 \\ \dot{\boldsymbol{X}}_2 = \boldsymbol{A}\boldsymbol{u} + \boldsymbol{B}\boldsymbol{X}_2 + \boldsymbol{D} + \boldsymbol{F}(t) \end{cases} \tag{36}$$

where $\boldsymbol{F}(t) = \begin{bmatrix} f_1(t) & f_2(t) & f_3(t) \end{bmatrix}^T$ is the external disturbance and linearization deviation in the formation control system.

To eliminate $\boldsymbol{F}(t)$, the non-homogeneous disturbance state observer with finite-time convergence is used to estimate $\boldsymbol{F}(t)$ in the system shown in (36). The specific form of the observer is [39]:

$$\begin{cases} \dot{z}_0 = v_0 + \boldsymbol{A}\boldsymbol{u} + \boldsymbol{B}\boldsymbol{X}_2 + \boldsymbol{D} \\ v_0 = -L^{\frac{1}{3}}\boldsymbol{\lambda}_2\boldsymbol{\xi}_0 \mathrm{sign}(z_0 - \boldsymbol{X}_2) - \boldsymbol{\mu}_2(z_0 - \boldsymbol{X}_2) + z_1 \\ \dot{z}_1 = v_1 \\ v_1 = -L^{\frac{1}{2}}\boldsymbol{\lambda}_1\boldsymbol{\xi}_1 \mathrm{sign}(z_1 - v_0) - \boldsymbol{\mu}_1(z_1 - v_0) + z_2 \\ \dot{z}_2 = -L\boldsymbol{\lambda}_0 \mathrm{sign}(z_2 - v_1) - \boldsymbol{\mu}_0(z_2 - v_1) \\ \hat{\boldsymbol{F}}(t) = z_1 \end{cases} \tag{37}$$

where $\boldsymbol{\lambda}_i = \mathrm{diag}(\lambda_{i1} \quad \lambda_{i2} \quad \lambda_{i3})$, $\lambda_{ij} > 0$, $i = 0, 1$, $2i = 0, 1, 2, j = 1, 2, 3$, $\boldsymbol{\mu}_i = \mathrm{diag}(\mu_{i1} \quad \mu_{i2} \quad \mu_{i3})$, $\mu_{ij} > 0, i = 0, 1, 2, j = 1, 2, 3$, $L > 0, z_0 = \mathrm{diag}(z_{01} \quad z_{02} \quad z_{03})$, $z_1 = \mathrm{diag}(z_{11} \quad z_{12} \quad z_{13})$, $z_2 = \mathrm{diag}(z_{21} \quad z_{22} \quad z_{23})$, $v_0 = \mathrm{diag}(v_{01} \quad v_{02} \quad v_{03})$, $v_1 = \mathrm{diag}(v_{11} \quad v_{12} \quad v_{13})$, $\boldsymbol{\xi}_0 = \mathrm{diag}\left(|z_{01} - x_2|^{\frac{2}{3}} \quad |z_{02} - x_4|^{\frac{2}{3}} \quad |z_{03} - x_6|^{\frac{2}{3}}\right)$, $\boldsymbol{\xi}_1 = \mathrm{diag}\left(|z_{11} - x_2|^{\frac{1}{2}} \quad |z_{12} - x_4|^{\frac{1}{2}} \quad |z_{13} - x_6|^{\frac{1}{2}}\right)$.

Surmise 1: The external disturbance and nonlinear error are bounded, that is

$$\tilde{\boldsymbol{F}}_1 \leq \boldsymbol{\Delta}_2 \tag{38}$$

where $\tilde{\boldsymbol{F}}_1 = \left[\left|f_1(t) - \hat{f}_1(t)\right| \quad \left|f_2(t) - \hat{f}_2(t)\right| \quad \left|f_3(t) - \hat{f}_3(t)\right|\right]^T$, $\boldsymbol{\Delta}_2 = (\Delta_{21} \quad \Delta_{22} \quad \Delta_{23})$, $\Delta_{2j} > 0, j = 1, 2, 3$.

Observing the system model shown in (36), we select the linear sliding mode to design the controller for the system. The specific form of the linear sliding mode surface is as follows:

$$\boldsymbol{s}_i = \boldsymbol{k}_{1i}\boldsymbol{X}_1 + \boldsymbol{k}_{2i}\boldsymbol{X}_2 + \boldsymbol{k}_{3i}\mathrm{sig}^{\alpha_i}(\boldsymbol{X}_1) \tag{39}$$

The derivative of the sliding mode surface can be obtained as

$$\begin{aligned} \dot{\boldsymbol{s}}_i &= \boldsymbol{k}_{1i}\dot{\boldsymbol{X}}_1 + \boldsymbol{k}_{2i}\dot{\boldsymbol{X}}_2 + \boldsymbol{k}_{3i}\alpha_i \left\|\boldsymbol{X}_1\right\|^{\alpha_i - 1}\dot{\boldsymbol{X}}_1 \\ &= \boldsymbol{k}_{1i}\boldsymbol{X}_2 + \boldsymbol{k}_{2i}\left(\boldsymbol{A}\boldsymbol{u} + \boldsymbol{B}\boldsymbol{X}_2 + \boldsymbol{D} + \boldsymbol{F}(t)\right) \\ &\quad + \boldsymbol{k}_{3i}\alpha_i \left\|\boldsymbol{X}_1\right\|^{\alpha_i - 1}\boldsymbol{X}_2 \end{aligned} \tag{40}$$

The choice of exponential approach is

$$\dot{\boldsymbol{s}}_i = -\boldsymbol{\varepsilon}_i \mathrm{sign}(\boldsymbol{s}_i) - \boldsymbol{k}_{4i}\boldsymbol{s}_i \tag{41}$$

For the sliding surface expressed in (39), we can design the controller as follows:

$$\begin{aligned} \boldsymbol{u}_i = \boldsymbol{A}^T(\boldsymbol{A}\boldsymbol{A}^T)^{-1}\boldsymbol{k}_{2i}^{-1}(&-\boldsymbol{\varepsilon}_i \mathrm{sign}(\boldsymbol{s}_i) - \boldsymbol{k}_{4i}\boldsymbol{s}_i \\ &- \boldsymbol{k}_{2i}\boldsymbol{D} - \boldsymbol{k}_{2i}\hat{\boldsymbol{\Delta}}_2\boldsymbol{\sigma}\,\mathrm{sign}(\boldsymbol{s}_i) - \boldsymbol{k}_{2i}\hat{\boldsymbol{F}}(t) \\ &- (\boldsymbol{k}_{1i} + \boldsymbol{k}_{3i}\alpha_i \left\|\boldsymbol{X}_1\right\|^{\alpha_i - 1} + \boldsymbol{k}_{2i}\boldsymbol{B})\boldsymbol{X}_2) \end{aligned} \tag{42}$$

where $\hat{\boldsymbol{\Delta}}_2$ is the estimated value of $\boldsymbol{\Delta}_2$; and $\boldsymbol{\sigma} = (\sigma_1 \quad \sigma_2 \quad \sigma_3)$, $\sigma_j > 1, j = 1, 2, 3$. The adaptive law is

$$\dot{\hat{\boldsymbol{\Delta}}}_2 = \boldsymbol{\varsigma}\boldsymbol{\sigma}^T \tag{43}$$

where $\boldsymbol{\varsigma} = \mathrm{diag}\left(|s_1| \quad |s_2| \quad |s_3|\right)$.

2) STABILITY ANALYSIS

Theorem 2: For the deduced formation model with disturbance in (36) under the condition of uncontrollable speed, we use the sliding mode surface in (39) and the reaching law in (41) to get the controller in (42) which can achieve and maintain formation.

Proof: Choosing a Lyapunov function

$$V_3 = \frac{1}{2}\boldsymbol{s}_i^T\boldsymbol{s}_i + \frac{1}{2}\tilde{\boldsymbol{\Delta}}_2^T\tilde{\boldsymbol{\Delta}}_2 \tag{44}$$

where $\tilde{\boldsymbol{\Delta}}_2 = \boldsymbol{\Delta}_2 - \hat{\boldsymbol{\Delta}}_2$, $\boldsymbol{\Delta}_2 = \begin{bmatrix} \Delta_2 & \Delta_2 & \Delta_2 \end{bmatrix}^T$. Differentiating V_3, we can get $\dot{V}_3$ as

$$\begin{aligned} \dot{V}_3 &= \boldsymbol{s}_i^T\dot{\boldsymbol{s}}_i + \tilde{\boldsymbol{\Delta}}_2^T\dot{\tilde{\boldsymbol{\Delta}}}_2 \\ &= \boldsymbol{s}_i^T\left(\boldsymbol{k}_{1i}\boldsymbol{X}_2 + \boldsymbol{k}_{2i}\left(\boldsymbol{A}\boldsymbol{u} + \boldsymbol{B}\boldsymbol{X}_2 + \boldsymbol{D} + \boldsymbol{F}(t)\right)\right. \\ &\quad \left. + \boldsymbol{k}_{3i}\alpha_i \left\|\boldsymbol{X}_1\right\|^{\alpha_i - 1}\boldsymbol{X}_2\right) - (\boldsymbol{\Delta}_2 - \hat{\boldsymbol{\Delta}}_2)^T\boldsymbol{\varsigma}\boldsymbol{\sigma}^T \\ &= \boldsymbol{s}_i^T\left(\boldsymbol{k}_{1i}\boldsymbol{X}_2 + \boldsymbol{k}_{2i}\boldsymbol{A}\boldsymbol{u} + \boldsymbol{k}_{2i}\left(\boldsymbol{B}\boldsymbol{X}_2 + \boldsymbol{D} + \boldsymbol{F}(t)\right)\right. \\ &\quad \left. + \boldsymbol{k}_{3i}\alpha_i \left\|\boldsymbol{X}_1\right\|^{\alpha_i - 1}\boldsymbol{X}_2\right) - (\boldsymbol{\Delta}_2 - \hat{\boldsymbol{\Delta}}_2)^T\boldsymbol{\varsigma}\boldsymbol{\sigma}^T \\ &= \boldsymbol{s}_i^T\left(\boldsymbol{k}_{1i}\boldsymbol{X}_2 - \boldsymbol{\varepsilon}_i \mathrm{sign}(\boldsymbol{s}_i) - \boldsymbol{k}_{4i}\boldsymbol{s}_i - \boldsymbol{k}_{1i}\boldsymbol{X}_2\right. \\ &\quad - \boldsymbol{k}_{2i}\left(\boldsymbol{B}\boldsymbol{X}_2 + \boldsymbol{D} + \boldsymbol{F}(t)\right) - \boldsymbol{k}_{3i}\alpha_i \left\|\boldsymbol{X}_1\right\|^{\alpha_i - 1}\boldsymbol{X}_2 \\ &\quad \left. + \boldsymbol{k}_{2i}\left(\boldsymbol{B}\boldsymbol{X}_2 + \boldsymbol{D} + \boldsymbol{F}(t)\right)\right) - (\boldsymbol{\Delta}_2 - \hat{\boldsymbol{\Delta}}_2)^T\boldsymbol{\varsigma}\boldsymbol{\sigma}^T \\ &= \boldsymbol{s}_i^T\left(-\boldsymbol{\varepsilon}_i \mathrm{sign}(\boldsymbol{s}_i) - \boldsymbol{k}_{4i}\boldsymbol{s}_i\right) - (\boldsymbol{\Delta}_2 - \hat{\boldsymbol{\Delta}}_2)^T\boldsymbol{\varsigma}\boldsymbol{\sigma}^T \\ &= \boldsymbol{s}_i^T\left(\boldsymbol{F}(t) - \hat{\boldsymbol{F}}(t) - \hat{\boldsymbol{\Delta}}_2\boldsymbol{\sigma}\,\mathrm{sign}(\boldsymbol{s}_i)\right. \\ &\quad \left. - \boldsymbol{\varepsilon}_i \mathrm{sign}(\boldsymbol{s}_i) - \boldsymbol{k}_{4i}\boldsymbol{s}_i\right) - (\boldsymbol{\Delta}_2 - \hat{\boldsymbol{\Delta}}_2)^T\boldsymbol{\varsigma}\boldsymbol{\sigma}^T \\ &= \boldsymbol{s}_i^T\boldsymbol{F}(t) - \boldsymbol{s}_i^T\hat{\boldsymbol{F}}(t) - \boldsymbol{s}_i^T\hat{\boldsymbol{\Delta}}_2\boldsymbol{\sigma}\,\mathrm{sign}(\boldsymbol{s}_i) \\ &\quad - \boldsymbol{s}_i^T\boldsymbol{\varepsilon}_i \mathrm{sign}(\boldsymbol{s}_i) - \boldsymbol{s}_i^T\boldsymbol{k}_{4i}\boldsymbol{s}_i - (\boldsymbol{\Delta}_2 - \hat{\boldsymbol{\Delta}}_2)^T\boldsymbol{\varsigma}\boldsymbol{\sigma}^T \\ &\leq \boldsymbol{s}_i^T\boldsymbol{\Delta}_2 - \boldsymbol{\Delta}_2^T\boldsymbol{\varsigma}\boldsymbol{\sigma}^T - \boldsymbol{s}_i^T\boldsymbol{\varepsilon}_i \mathrm{sign}(\boldsymbol{s}_i) - \boldsymbol{s}_i^T\boldsymbol{k}_{4i}\boldsymbol{s}_i \\ &\leq \boldsymbol{\Delta}_2^T\boldsymbol{\varsigma}\boldsymbol{\sigma}^T - \boldsymbol{\Delta}_2^T\boldsymbol{\varsigma}\boldsymbol{\sigma}^T - \boldsymbol{s}_i^T\boldsymbol{\varepsilon}_i \mathrm{sign}(\boldsymbol{s}_i) - \boldsymbol{s}_i^T\boldsymbol{k}_{4i}\boldsymbol{s}_i \\ &= \boldsymbol{\Delta}_2^T\boldsymbol{\varsigma}(\boldsymbol{I}_{3\times 1} - \boldsymbol{\sigma}^T) - \boldsymbol{s}_i^T\boldsymbol{\varepsilon}_i \mathrm{sign}(\boldsymbol{s}_i) - \boldsymbol{s}_i^T\boldsymbol{k}_{4i}\boldsymbol{s}_i \\ &\leq -\boldsymbol{s}_i^T\boldsymbol{\varepsilon}_i \mathrm{sign}(\boldsymbol{s}_i) - \boldsymbol{s}_i^T\boldsymbol{k}_{4i}\boldsymbol{s}_i \end{aligned} \tag{45}$$

Observing the (45), due to

$$\mathrm{sign}(s)s = \begin{cases} s, & s > 0 \\ -s, & s < 0 \end{cases} \tag{46}$$

and since $\boldsymbol{\varepsilon}_i > 0$ and $\boldsymbol{k}_{4i} > 0$, we can get

$$\boldsymbol{s}_i^T\boldsymbol{\varepsilon}_i \mathrm{sign}(\boldsymbol{s}_i) \geq 0 \tag{47}$$

$$\boldsymbol{s}_i^T\boldsymbol{k}_{4i}\boldsymbol{s}_i \geq 0 \tag{48}$$

So according to the proof of $\dot{V}_1 < 0$, it can be obtained that $\dot{V}_3 < 0$, and the system state can reach the sliding surface. According to the Lyapunov stability theory, the system is asymptotically stable. The sliding mode surface $\boldsymbol{s}_i$ designed in this article can converge to zero in the finite time. After convergence, the system state is

$$\boldsymbol{k}_{1i}\boldsymbol{X}_1 + \boldsymbol{k}_{2i}\boldsymbol{X}_2 + \boldsymbol{k}_{3i}\mathrm{sig}^{\alpha_i}(\boldsymbol{X}_1) = \boldsymbol{s}_i = \boldsymbol{0} \tag{49}$$

The state equation of the system can be organized as

$$\boldsymbol{X}_2 = \boldsymbol{k}_{2i}^{-1}(-\boldsymbol{k}_{1i}\boldsymbol{X}_1 - \boldsymbol{k}_{3i}\mathrm{sig}^{\alpha_i}(\boldsymbol{X}_1)) \tag{50}$$

Choosing another Lyapunov function

$$V_4 = \frac{1}{2}\boldsymbol{X}_1^T\boldsymbol{X}_1 \tag{51}$$

and differentiating (51), the result is

$$\begin{aligned}\dot{V}_4 &= \boldsymbol{X}_1^T\dot{\boldsymbol{X}}_1 = \boldsymbol{X}_1^T\boldsymbol{X}_2 \\ &= \boldsymbol{X}_1^T\boldsymbol{k}_{2i}^{-1}(-\boldsymbol{k}_{1i}\boldsymbol{X}_1 - \boldsymbol{k}_{3i}\mathrm{sig}^{\alpha_i}(\boldsymbol{X}_1)) \\ &= -\boldsymbol{k}_{2i}^{-1}\boldsymbol{k}_{1i}\boldsymbol{X}_1^T\boldsymbol{X}_1 - \boldsymbol{k}_{2i}^{-1}\boldsymbol{k}_{3i}\boldsymbol{X}_1^T\mathrm{sig}^{\alpha_i}(\boldsymbol{X}_1) \\ &= -\boldsymbol{k}_{2i}^{-1}\boldsymbol{k}_{1i}\boldsymbol{X}_1^T\boldsymbol{X}_1 - \boldsymbol{k}_{2i}^{-1}\boldsymbol{k}_{3i}\boldsymbol{X}_1^T\,\|\boldsymbol{X}_1\|^{\alpha_i}\,\mathrm{sign}(\boldsymbol{X}_1) \\ &= -\boldsymbol{k}_{2i}^{-1}\boldsymbol{k}_{1i}\,\|\boldsymbol{X}_1\| - \boldsymbol{k}_{2i}^{-1}\boldsymbol{k}_{3i}\,\|\boldsymbol{X}_1\|^{\alpha_i+1} \\ &\le 0\end{aligned} \tag{52}$$

According to the principle of invariance, we can know $\dot{V}_4 < 0$, so the system state can converge. According to the Lyapunov stability theory, the system is gradually stable, which means when $t \to \infty, \boldsymbol{X}_1 \to 0$.

$$\begin{cases}\lim\limits_{t\to\infty}\Delta X_i = x_i^* \\ \lim\limits_{t\to\infty}\Delta Y_i = y_i^* \\ \lim\limits_{t\to\infty}\Delta Z_i = z_i^*\end{cases} \tag{53}$$

According to (53), the position difference ΔX_i, ΔY_i and ΔZ_i can converge to the expected value in each axis, respectively.

Note that the guidance law function shown in (42) has a sign function term. To reduce chattering, the sign function is replaced with a saturation function, and the controller can be rewritten as

$$\begin{aligned}\boldsymbol{u}_i = \boldsymbol{A}^T(\boldsymbol{A}\boldsymbol{A}^T)^{-1}\boldsymbol{k}_{2i}^{-1}(&-\boldsymbol{\varepsilon}_i\mathrm{sat}(\boldsymbol{s}_i) - \boldsymbol{k}_{4i}\boldsymbol{s}_i \\ &- \boldsymbol{k}_{2i}\boldsymbol{D} - \boldsymbol{k}_{2i}\hat{\boldsymbol{\Delta}}_2\boldsymbol{\sigma}\,\mathrm{sat}(\boldsymbol{s}_i) - \boldsymbol{k}_{2i}\hat{\boldsymbol{F}}(t) \\ &- (\boldsymbol{k}_{1i} + \boldsymbol{k}_{3i}\alpha_i\,\|\boldsymbol{X}_1\|^{\alpha_i-1} + \boldsymbol{k}_{2i}\boldsymbol{B})\boldsymbol{X}_2)\end{aligned} \tag{54}$$

Remark: The adjustment rule of parameters

The control algorithm designed in this article includes many parameters. We choose some important parameters to discuss the adjustment rule of parameters, including $\alpha_i, \boldsymbol{k}_{1i}, \boldsymbol{k}_{2i}$.

α_i*:* The value range of α_i is $1 < \alpha_i < 2$. We take a point between 1.1 and 1.9 for each 0.1 to conduct simulation verification. It is found that 1.2 is the best for the effect of the control system. The change of the value will make the control performance bad.

$\boldsymbol{k}_{1i}$*:* We adjust the three parameters in $\boldsymbol{k}_{1i}$ and carry out many simulations. Results show that the error of formation control system is the smallest when $\boldsymbol{k}_{1i} = \mathrm{diag}[\,0.8\ \ 16.5\ \ 0.5\,3\,]$.

$\boldsymbol{k}_{2i}$*:* We adjust the three parameters in $\boldsymbol{k}_{2i}$ and carry out many simulations. Results show that the error of formation control system is the smallest when $\boldsymbol{k}_{2i} = \mathrm{diag}\left[\,1\ \ 1.2\ \ 1\,\right]$.

The parameters $\boldsymbol{k}_{1i}$ and $\boldsymbol{k}_{2i}$ do not have clear range, and are only required to be positive. Therefore, we have not enough guidance on parameter selection and can only test through simulations.

TABLE 1. Initial parameter values of missiles.

Missile	Leader	Follower1	Follower2
Coordinate value (km)	(22,5,6.36)	(8,8.66,0)	(28.64,9.17,0)
Ballistic inclination angle (°)	30	15	15
Ballistic deflection angle (°)	0	10	10
Speed (m / s)	1000	1000	1000

IV. SIMULATIONS

To verify the quality of the control method proposed in this article for the formation of missiles with uncontrollable speed, four simulation experiments are designed in this article. In the simulation Scenario 1 - Scenario 3, we use the formation model without disturbances and linearization deviations. The purpose of Scenario 1 is to verify the effectiveness and feasibility of the formation control system. The purpose of Scenario 2 is to verify the ability of dealing with the measuring noise of the system. The purpose of Scenario 3 is to verify that the formation control system applies to various formations. In Scenario 4, we use the formation control system with disturbances and linearization deviations. Its purpose is to verify that the formation control system has a better anti-disturbance effect.

We use one leader and two followers to form the formation. The leader is going to attack the virtual target during the mid-guidance stage. It is required that the two followers form the desired formation with the leader in the finite time. The initial parameter values of the missiles are shown in Table 1. It is assumed that the virtual target is located at (0, 5000, 0)m and is stationary, and the speed of the leader and two followers are all 1000m/s and remain unchanged. The maximum amplitude of acceleration is $A_M = 40$g and the simulation step size is 0.001s. We choose MATLAB as the simulation software.

For the three missiles shown in Table 1, the sliding mode coefficients of the leader are selected as follows: $m = 5$, $n = 10$, and $\delta_1 = \delta_2 = 0.0025$. The parameter values of the followers are as follows: $\alpha_1 = \alpha_2 = 1.2$, $\gamma_1 = \gamma_2 = 0.6$, $\boldsymbol{k}_{1i} = \mathrm{diag}[\,0.8\ \ 16.5\ \ 0.5\,3\,]$, $\boldsymbol{k}_{2i} = \mathrm{diag}\left[\,1\ \ 1.2\ \ 1\,\right]$, $\boldsymbol{k}_{3i} = \mathrm{diag}[\,0.01\ \ 0.01\ \ 0.01\,]$, $\boldsymbol{k}_{4i} = \mathrm{diag}[\,13\ \ 0.02\ \ 10\,]$, $\boldsymbol{\varepsilon}_i = [\,1\ \ 1.1\ \ 0.8\,]$, and $i = 1, 2$. The parameters in the saturation function are selected as $\sigma_1 = \sigma_2 = 0.01$. In the following work, we perform four simulation experiments.

Scenario 1: Expect the three missiles to form a one-line formation. That is, the expected position difference between the leader and the first follower is $x_1^* = 0$m, $y_1^* = 0$m, $z_1^* = 8000$m, and the expected position difference between the leader and the second follower is $x_2^* = 0$m, $y_2^* = 0$m, $z_2^* = -8000$m. Simulation results of the control law in (34) are

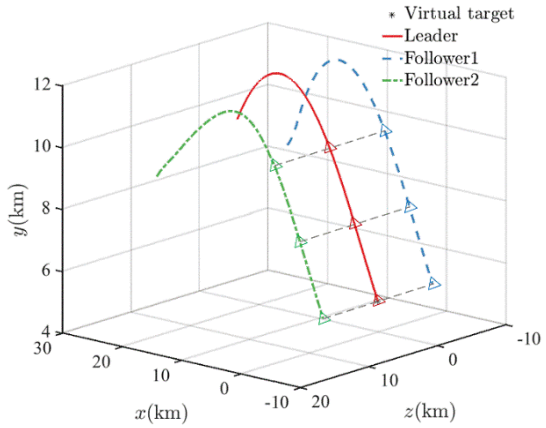

FIGURE 7. Three missiles' trajectory under the algorithm proposed in this article.

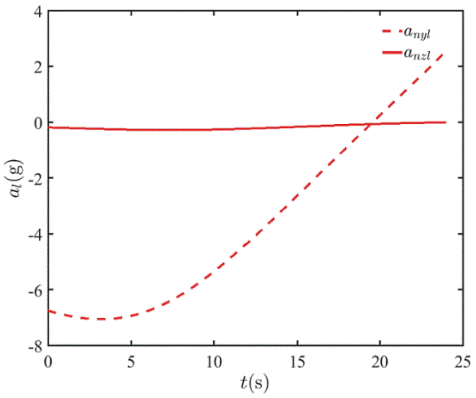

FIGURE 8. Acceleration curves of the leader.

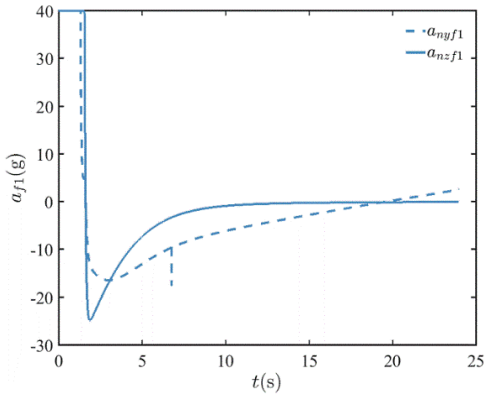

FIGURE 9. Acceleration curves of the first follower.

shown in Figs. 7-12. The error of the relative position between the leader and the follower in the same initial condition is shown in Table 2. To prove the feasibility of the method proposed in this article, we compare it with an existing method using autopilot from [20]. Simulation results of the existing method are shown in Figs. 13-21. The position error of the two methods is shown in Table 2, and the convergence time is shown in Table 3.

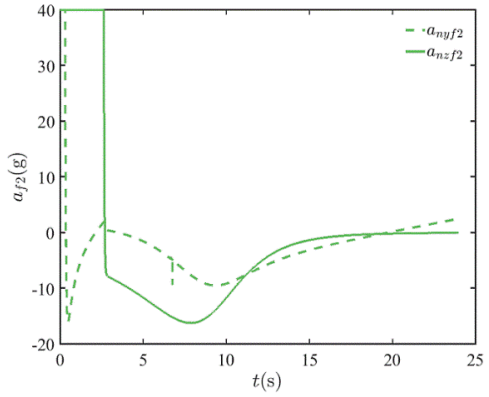

FIGURE 10. Acceleration curves of the second follower.

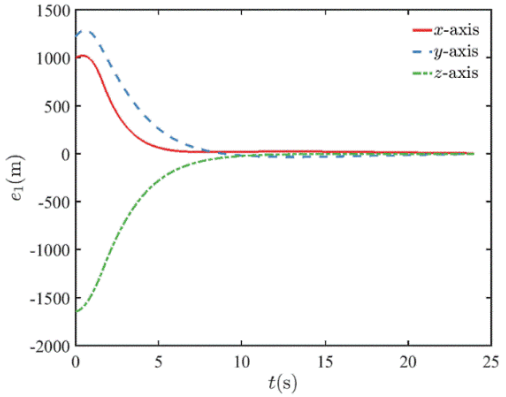

FIGURE 11. Relative position error of the leader and the first follower in three axes.

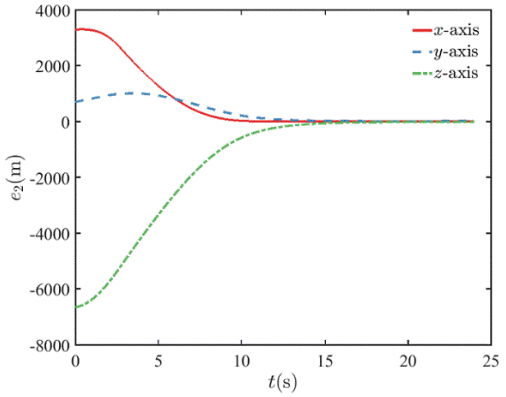

FIGURE 12. Relative position error of the leader and the second follower in three axes.

TABLE 2. Relative position error information.

Axis in inertial coordinate system	e_{1T}(m)	e_{2T}(m)	e_1(m)	e_2(m)
x	0.8	5	6.6	24.4
y	17	28	0.1	30.6
z	0	0	0.07	0.4

The leader uses a guidance law designed with the sliding mode variable structure control theory to attack the virtual target. So, as shown in Fig. 7, it can be seen that the trajectories

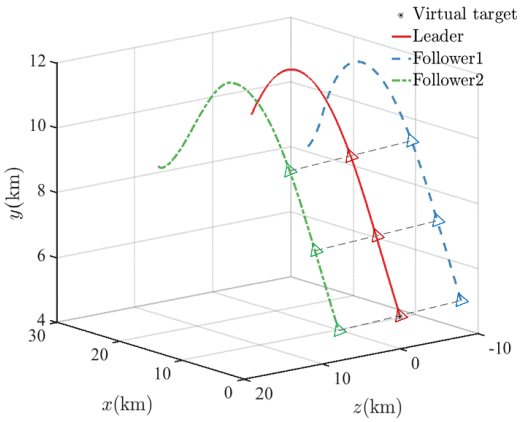

FIGURE 13. Three missiles' trajectory of the existing algorithm [20].

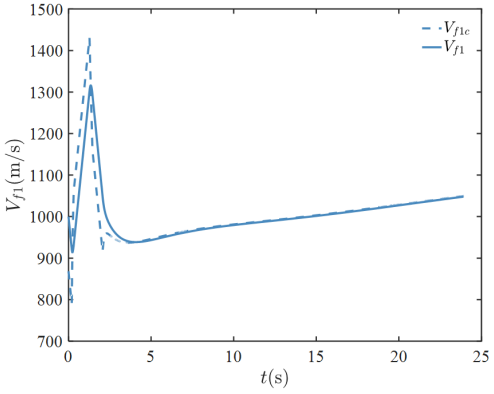

FIGURE 14. Speed tracking curves of the first follower [20].

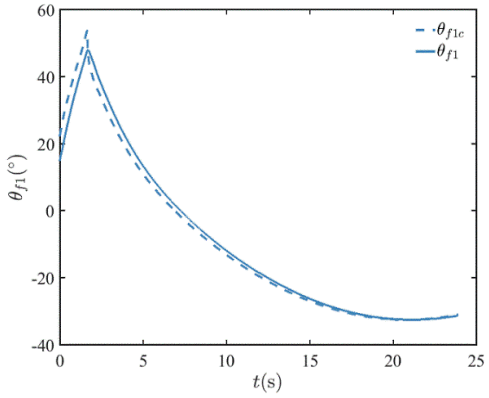

FIGURE 15. Ballistic inclination angle tracking curves of the first follower [20].

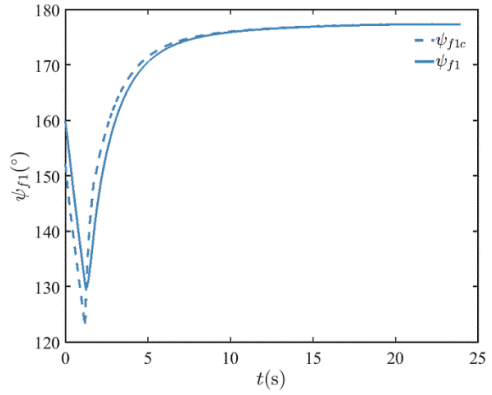

FIGURE 16. Ballistic deflection angle tracking curves of the first follower [20].

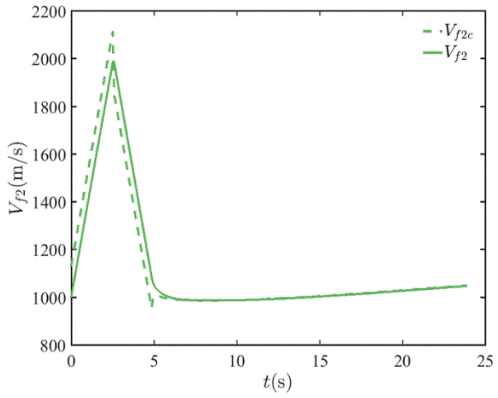

FIGURE 17. Speed tracking curves of the second follower [20].

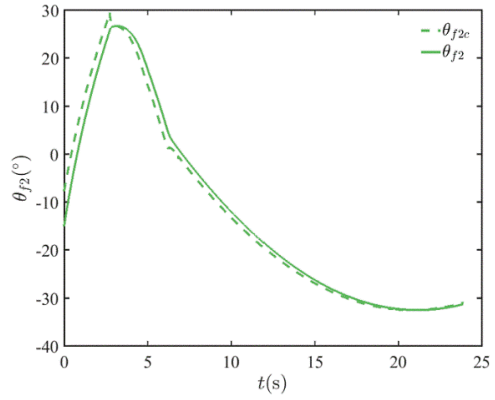

FIGURE 18. Ballistic inclination angle tracking curves of the second follower [20].

are smoother and there is no large curvature. The acceleration of the leader is shown in Fig. 8, where the curves of the pitch channel and the yaw channel are smooth. In Fig. 7, the curves of the two followers change rapidly in the initial stage and reach the expected value within a limited time, then those curves become smooth. This is reflected in Fig. 9 and Fig. 10, where the acceleration curves of the two followers change drastically in the initial stage, and when the formation requirements are met, the curves become smooth.

Fig. 11 and Fig. 12 show the difference between the actual and expected distance of the leader and each follower, respectively. The difference is named as the relative position error. It is shown that the error of the two followers will reach zero within a limited time. Table 2 shows that steady-state formation errors of the follower are relatively small, considering that the maximum error is 30.6m and the speed is 1000m/s. This indicates that the formation control system designed in this article is feasible. More importantly, the control system does not need to control the speed of the missile, which is more in line with practical requirements.

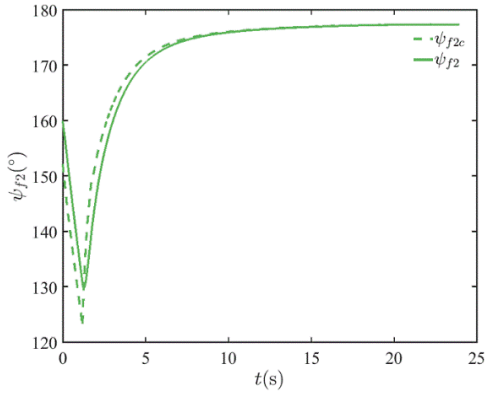

FIGURE 19. Ballistic deflection angle tracking curves of the second follower [20].

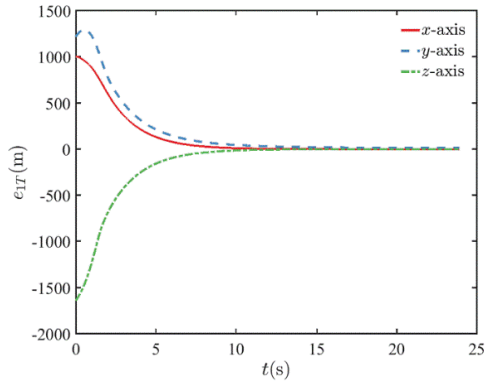

FIGURE 20. Relative position error of the leader and the first follower in three axes [20].

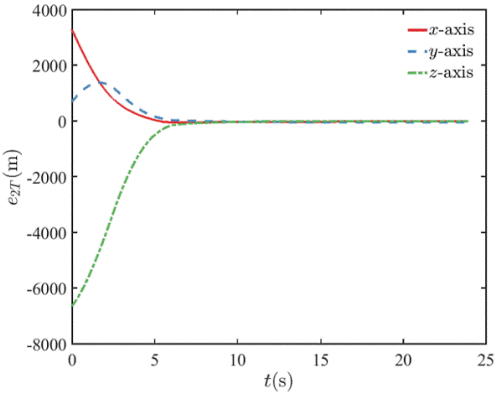

FIGURE 21. Relative position error of the leader and the second follower in three axes [20].

As shown in Fig. 13, the existing autopilot-based formation controller design can realize and maintain the formation, and the trajectory is smooth. It can be seen from Fig. 14 to Fig. 19 that the control input of the two followers can keep up with the control commands within a limited time to meet the formation requirements. As shown in Fig. 20 and Fig. 21, the relative position error of the two followers and the leader can both approach zero within a finite time. As it is shown in Table 2, the maximum steady-state error of the two followers is 28m, which is relatively small. But the disadvantage of this method is that it requires the speed of the missile to be completely controllable in real time, which is difficult to achieve in reality.

TABLE 3. Convergence time information.

Axis in inertial coordinate system	t_{fiT}(s)	t_{f_2T}(s)	t_{f_1}(s)	t_{f2}(s)
x	6.012	4.807	4.752	9.278
y	7.866	5.615	6.937	12.473
z	6.368	7.093	7.516	13.936

To analyze the convergence performance, the convergence time of the two followers is recorded. Since the expected position value in the x and y axis is zero, and it is inconvenient to use them to express convergence, we take $0-1\%$ of the expected value in the $z-$ axis as the width of convergence zone in all three axes. The time for the two followers to reach the convergence zone is shown in Table 3. The convergence time of the existing method is also given in Table 3.

In Table 3, t_{fiT} is the time used by the two followers to reach the convergence zone using the existing method; and t_{fi} is the time for the *ith* follower to reach the convergence zone using the method proposed in this article. It can be seen that the maximum t_{fiT} of two followers in three axes is 7.866s, and the total simulation time is 23.975s. This means that both followers can converge within 35% of the total simulation time. And the maximum t_{fi} is 13.936s, which means both followers can converge within 60% of the total simulation time. Therefore, the existing method [20] converges faster. It must take less time to reach the convergence zone because the speed is controllable.

Scenario 2: Considering there are measurement noises in the system in practice, we add the measurement noise $\boldsymbol{\omega}(t)$ to system in (13), and get the new form of the system as

$$\begin{cases} \dot{\boldsymbol{X}}_1 = \boldsymbol{X}_2 \\ \dot{\boldsymbol{X}}_2 = \boldsymbol{A}\boldsymbol{u} + \boldsymbol{B}\boldsymbol{X}_2 + \boldsymbol{D} + \boldsymbol{\omega}(t) \end{cases} \tag{55}$$

where $\boldsymbol{\omega}(t) = \text{diag}[10\text{rand}(), 10\text{rand}(), 10\text{rand}()]$.

The linear sliding mode surface as shown in (16) is adopted to design the formation controller. The final expression of the controller is as follows:

$$\begin{aligned} \boldsymbol{u}_i = \boldsymbol{A}^T(\boldsymbol{A}\boldsymbol{A}^T)^{-1}\boldsymbol{k}_{2i}^{-1}(-\boldsymbol{\varepsilon}_i\text{sign}(\boldsymbol{s}_i) - \boldsymbol{k}_{4i}\boldsymbol{s}_i \\ - \boldsymbol{k}_{2i}\boldsymbol{D} - \boldsymbol{k}_{2i}\boldsymbol{\omega}(t) - (\boldsymbol{k}_{1i} + \boldsymbol{k}_{3i}\alpha_i \|\boldsymbol{X}_1\|^{\alpha_i - 1} + \boldsymbol{k}_{2i}\boldsymbol{B})\boldsymbol{X}_2) \end{aligned} \tag{56}$$

The same initial condition as that in scenario 1 is used, where missiles are commanded to form a one-line formation. The expected position difference between the leader and the first follower is $x_1^* = 0$m, $y_1^* = 0$m, $z_1^* = 8000$m, and the difference between the leader and the second follower is $x_2^* = 0$m, $y_2^* = 0$m, $z_2^* = -8000$m. Simulation results using the control law shown in (56) are shown in Figs. 22-24.

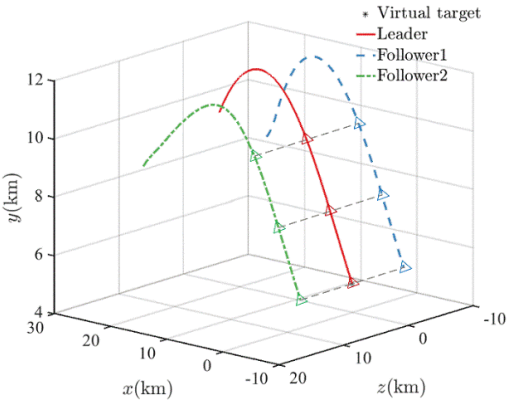

FIGURE 22. Three missiles' trajectory under the algorithm proposed in this article.

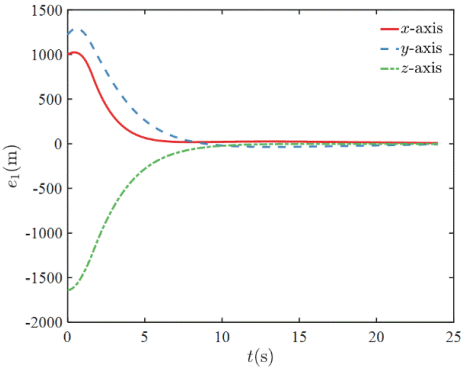

FIGURE 23. Relative position error of the leader and the first follower in three axes.

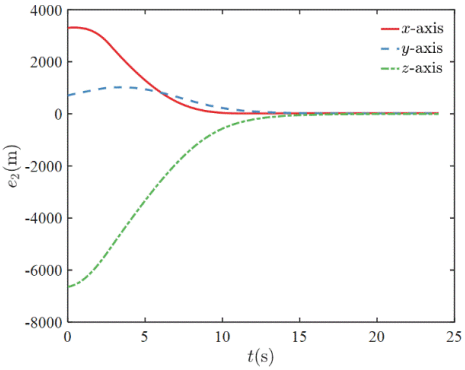

FIGURE 24. Relative position error of the leader and the second follower in three axes.

TABLE 4. Relative position error information.

Axis in inertial coordinate system	e_1(m)	e_2(m)
x	7.1	23.2
y	7.1	23.3
z	1.5	2.0

The relative position error of the leader and the followers is shown in Table 4.

Table 2 shows the simulation results not considering measurement noises, and Table 4 shows the simulation results considering measurement noises. Comparing the results in

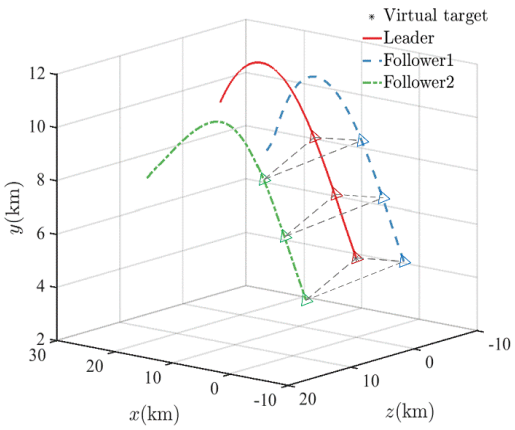

FIGURE 25. Three missiles' trajectory under the algorithm proposed in this article.

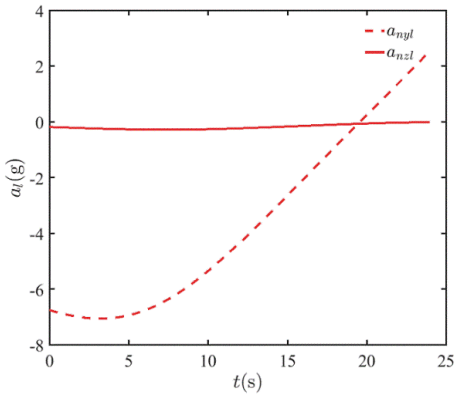

FIGURE 26. Acceleration curves of the leader.

TABLE 5. Relative position error information.

Axis in inertial coordinate system	e_1(m)	e_2(m)
x	6.2	24.4
y	17	30.6
z	0.05	0.4

the two tables, it can be found that when the measurement noise is added, the error in the z direction increases, but the error in the x and y directions either increases or decreases. So, the effect of measurement noises on the design of our formation controller is found to be insignificant.

Scenario 3: To verify the formation adaptability of the design method in this article, a simulation of another formation is given below. It is expected that the three missiles will form a triangular formation, that is, the expected position difference between the leader and the first follower is $x_1^* = 0$m, $y_1^* = 1000$m, $z_1^* = 8000$m, and the expected position difference between the leader and the second follower is $x_2^* = 0$m, $y_2^* = 1000$m, $z_2^* = -8000$m. Using (34), simulation results are shown in Figs. 25-30. Relative position errors are shown in Table 5.

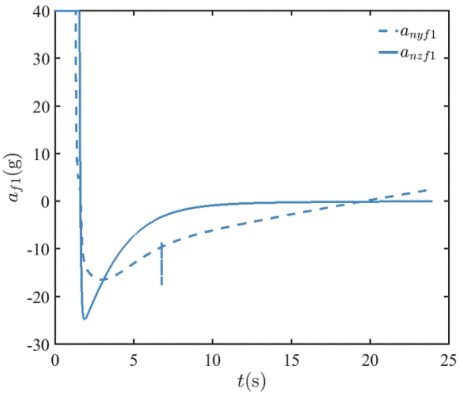

FIGURE 27. Acceleration curves of the first follower.

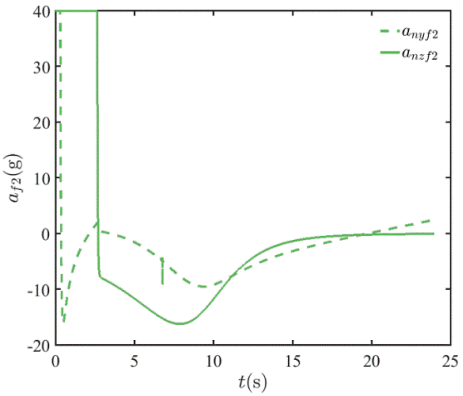

FIGURE 28. Acceleration curves of the second follower.

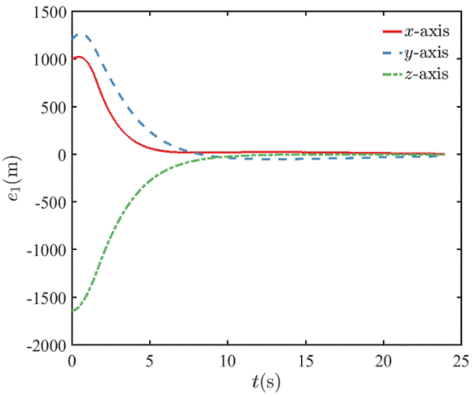

FIGURE 29. Relative position error of the leader and the first follower in three axes.

As shown in Fig. 25, the leader's overall trajectory is smooth. Observing the acceleration curves of the leader shown in Fig. 26, the pitch channel and yaw channel curves are smooth. The curves of the two followers change rapidly at the initial stage and reach the expected value within a limited time, then become smooth. Corresponding features can be found in the acceleration curves of the two followers in Fig. 27 and Fig. 28. The curves change drastically in the initial stage, and become smooth when the formation requirements are met.

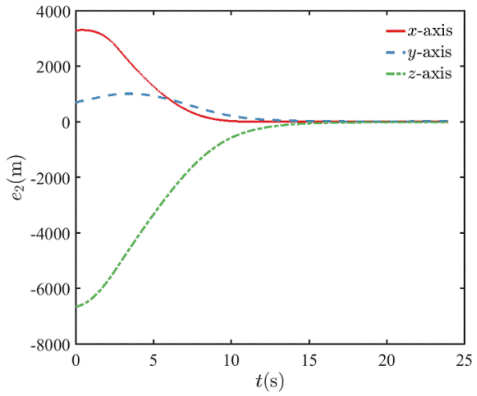

FIGURE 30. Relative position error of the leader and the second follower in three axes.

TABLE 6. Convergence time information.

Axis in inertial coordinate system	t_{f_1}(s)	t_{f2}(s)
x	5.396	9.777
y	7.125	13.832
z	7.514	13.936

TABLE 7. Relative position error information.

Axis in inertial coordinate system	e_1(m)	e_2(m)
x	6.47	32.70
y	1.39	21.88
z	0.07	0.73

Fig. 29 and Fig. 30 show the relative position error between the leader and each follower, respectively. It can be found that both followers can reach zero errors within a limited time. Table 5 shows that the tracking errors of the two followers are relatively small, considering that the maximum error is 30.6m and the speed is 1000m/s. This indicates that the formation controller designed in this article has good precision. Compared with the one-line simulation, the error did not increase, indicating the method has good formation adaptability.

In this Scenario, the expected value of $0-5\%$ in the x and y axis and $0-1\%$ in the $z-$axis are taken as the convergence zone in the axis, respectively. The time for the two followers to reach the convergence zone is shown in Table 6.

It can be seen from Table 6 that the maximum convergence time is 13.936s, and the total simulation time is 23.975s. So the convergence of the two followers happens within 60% of the total time.

Scenario 4: To verify the anti-disturbance ability of the design method in this article, another simulation is done. Based on the formation in Scenario 3, we add a disturbance item $\boldsymbol{F}(t) = \left(\sin(0.5t)\ \sin(0.5t)\ \sin(0.5t)\right)^T$ into the model. Using (54), the simulation results are shown in Figs. 31-38. The relative position error is shown in Table 7.

Comparing Fig. 31 with Fig. 25, it can be found that for the two conditions, the trajectories of the three missiles do not change much. Comparing Figs. 32-34 with Figs. 26-28,

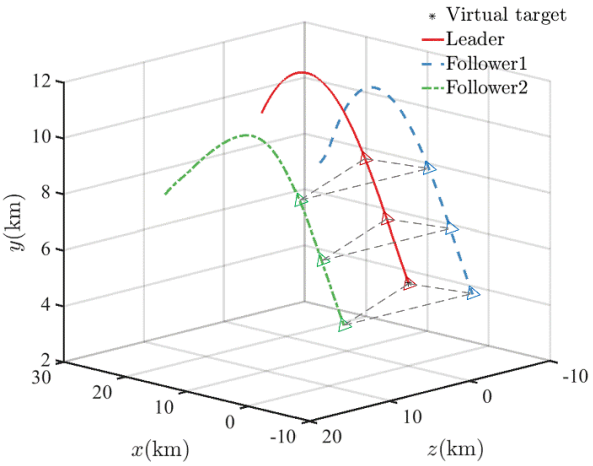

FIGURE 31. Three missiles' trajectory under the algorithm proposed in this article.

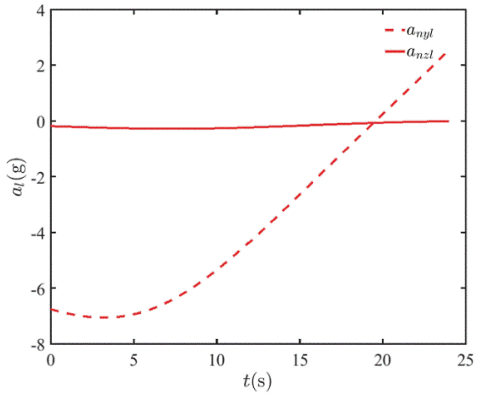

FIGURE 32. Acceleration curves of the leader.

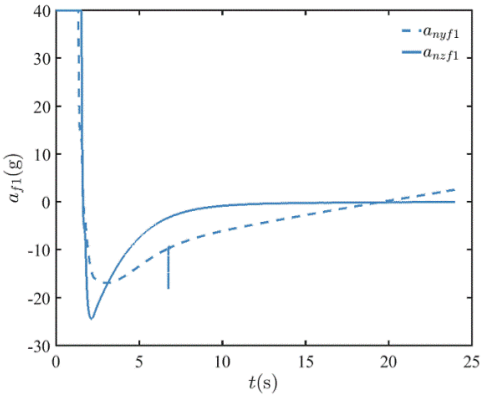

FIGURE 33. Acceleration curves of the first follower.

we know that the acceleration curves of the three missiles show some fluctuations, but all within an acceptable range. Observing Fig. 35 and Fig. 36, it can be found that the observation error of disturbances in the two followers will converge to zero within a limited time. By combining Fig. 37 and Fig. 38 with Table 7, it can be found that the tracking error of the two followers is not much different from that in Scenario 3.

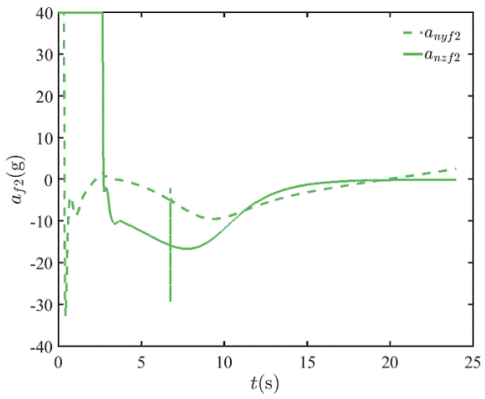

FIGURE 34. Acceleration curves of the second follower.

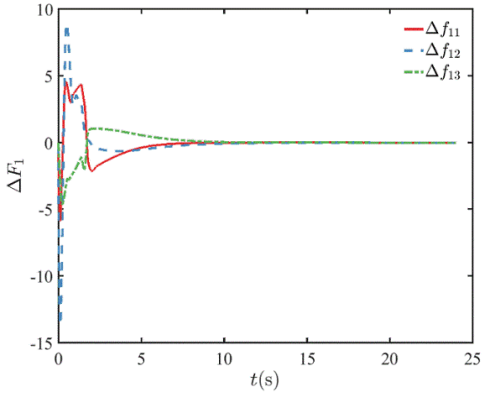

FIGURE 35. Observation error of disturbances of the first follower.

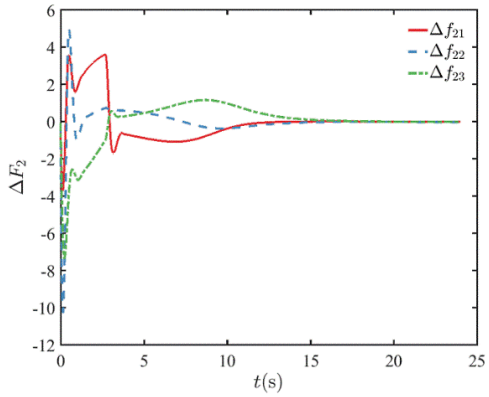

FIGURE 36. Observation error of disturbances of the second follower.

The above analysis shows that the formation control system designed in this article can cope with external disturbances and linearization errors.

Note: Based on the four Scenarios above, we compare the formation control system from [20] and the formation control system of this article. The details are shown in Table 8.

From Table 8, the existing method considers the real-time controllability of speed, but this article does not consider it, which is more in line with realistic requirements. The two methods both have a small maximum formation error, and the absolute value is close. On model complexity, in the

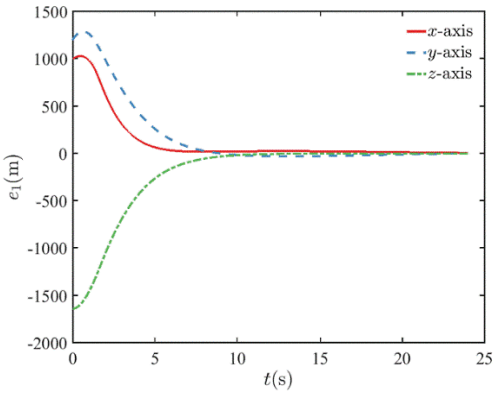

FIGURE 37. Relative position error of the leader and the first follower in three axes.

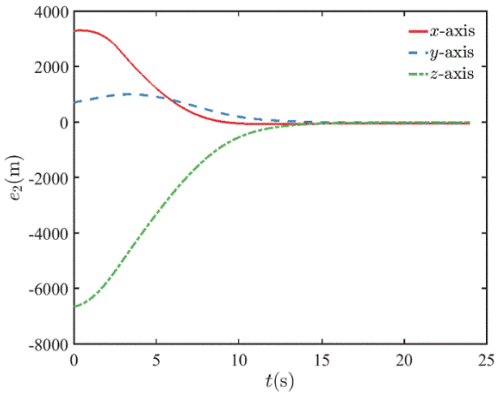

FIGURE 38. Relative position error of the leader and the second follower in three axes.

TABLE 8. Comparison of two formation control systems.

	From [20]	Of this paper
Controlled variable	V	V(const)
Maximum formation error	28m	30.6m
Model complexity	High	Low
Anti-measurement-noise ability	Unverified	Strong
Formation adaptability	Unverified	High
Anti-disturbance ability	Weak	Strong

method from [20], the expected relative position is expressed under the relative coordinate system between the leader and the follower. So it requires the second-order derivative of the product of the coordinate transformation matrix and the expected relative position, which is complex. Instead, using the inertial coordinate system for expression, the method in this article does not need to take the derivative, which can simplify the computation. And the most important is that the anti-disturbance ability of this method is better than the existing method. This is because the existing method is based on the back-stepping method, but our method adopts the sliding mode variable structure control theory which is superior in the anti-disturbance ability. Verified by the two different formations in simulation, our method has good formation adaptability. At last, simulation results verify the strong anti-measurement-noise ability of our method.

In summary, the formation control system proposed in this article has better versatility, lower complexity, stronger robustness and formation adaptability, according to the theoretical analysis and simulations.

V. CONCLUSION

Under the premise that the speed of the missile is not controllable, we adopt the Leader-Follower formation mode to design the formation control system.

First, the model of the formation control problem is constructed in Section 2. We describe the expected relative position in the inertial coordinate system; then we design the model of the problem in the inertial coordinate system; then we transform the model into the ballistic coordinate system, and by reasoning and conversion, the model needed is obtained.

Next, in Section 3, for the different cases where disturbances are ignored or considered, the formation controller of the leader and the follower is designed based on the sliding mode variable structure control theory, and the stability of the controller is proved by the Lyapunov stability theory.

Finally, four simulation experiments are done in Section 4. Without considering the disturbances, we design a one-line formation in Scenario 1 and Scenario 2, and a triangular formation in Scenario 3. In Scenario 1, we compare our method with an existing method [20]. In Scenario 2, the ability of our method to overcome measurement noises is verified. Considering the disturbances, we design Scenario 4 using the same formation as that of Scenario 3. Simulation results show that the formation control system proposed in this article has better versatility, easier computation, stronger robustness and stronger formation adaptability. Moreover, the formation controller proposed in this article does not require controllable speed, which is more convenient to be applied in practice.

VI. FUTURE RECOMMENDATION

According to the control system design process in this article and the control system designed in an existing literature, we present that the research direction to further improve the work mainly includes:

(1) In the design of multi-missile formation control system, communication delay and other practical factors should be considered;
(2) The way to further reduce the complexity of algorithm design;
(3) The way to further improve the convergence speed and accuracy of the control algorithm.

REFERENCES

[1] *World Missile Encyclopedia' Revision Committee.: 'World Missile Encyclopedia*, 3th ed, Military Science Press, Beijing, China, 2013.
[2] T. Han, Z.-H. Guan, R.-Q. Liao, J. Chen, M. Chi, and D.-X. He, "Distributed finite-time formation tracking control of multi-agent systems via FTSMC approach," *IET Control Theory Appl.*, vol. 11, no. 15, pp. 2585–2590, Oct. 2017.

[3] Y. Huang, W. Liu, B. Li, Y. Yang, and B. Xiao, "Finite-time formation tracking control with collision avoidance for quadrotor UAVs," *J. Franklin Inst.*, vol. 357, no. 7, pp. 4034–4058, May 2020.
[4] H. Rezaee, F. Abdollahi, and H. A. Talebi, "$\mathcal{H}_\infty$ based motion synchronization in formation flight with delayed communications," *IEEE Trans. Ind. Electron.*, vol. 61, no. 11, pp. 6175–6182, Nov. 2014.
[5] H. Du, W. Zhu, G. Wen, and D. Wu, "Finite-time formation control for a group of quadrotor aircraft," *Aerosp. Sci. Technol.*, vol. 69, pp. 609–616, Oct. 2017.
[6] A. Ajorlou, K. Moezzi, A. G. Aghdam, S. Tafazoli, and S. G. Nersesov, "Two-stage energy-optimal formation reconfiguration strategy," *Automatica*, vol. 48, no. 10, pp. 2587–2591, Oct. 2012.
[7] A. Ajorlou, K. Moezzi, A. G. Aghdam, and S. G. Nersesov, "Two-stage time-optimal formation reconfiguration strategy," *Syst. Control Lett.*, vol. 62, no. 6, pp. 496–502, Jun. 2013.
[8] W. Zhao and T. H. Go, "Quadcopter formation flight control combining MPC and robust feedback linearization," *J. Franklin Inst.*, vol. 351, no. 3, pp. 1335–1355, Mar. 2014.
[9] Y. Xu and Z. Zhen, "Multivariable adaptive distributed leader-follower flight control for multiple UAVs formation," *Aeronaut. J.*, vol. 121, no. 1241, pp. 877–900, Jul. 2017.
[10] Z. Zhen, G. Tao, Y. Xu, and G. Song, "Multivariable adaptive control based consensus flight control system for UAVs formation," *Aerosp. Sci. Technol.*, vol. 93, Oct. 2019, Art. no. 105336.
[11] B. Yan, P. Shi, C. C. Lim, C. Wu, and Z. Shi, "Optimally distributed formation control with obstacle avoidance for mixed-order multi-agent systems under switching topologies," *IET Control Theory Appl.*, vol. 12, no. 13, pp. 1835–1863, 2018.
[12] X. Wang, D. Liu, and Z. Tian, "A composite formation strategy for multiple missiles," in *Proc. 3rd Int. Conf. Control, Autom. Robot. (ICCAR)*, Apr. 2017, pp. 684–691.
[13] C. Wei, J. Guo, B. Lu, Y. Shen, and L. Zhang, "Adaptive control for missile formation keeping under leader information unavailability," in *Proc. 10th IEEE Int. Conf. Control Autom. (ICCA)*, Jun. 2013, pp. 902–907.
[14] C. Wei, J. Guo, S.-Y. Park, J. Xu, and X. Ma, "IFF optimal control for missile formation reconfiguration in cooperative engagement," *J. Aerosp. Eng.*, vol. 28, no. 3, May 2015, Art. no. 04014087.
[15] C. Wei, Y. Shen, X. Ma, J. Guo, and N. Cui, "Optimal formation keeping control in missile cooperative engagement," *Aircr. Eng. Aerosp. Technol.*, vol. 84, no. 6, pp. 376–389, Oct. 2012.
[16] J. Ma, Q. H. Ma, and G. Wang, "Optimal reconstruction control of missile formation based on pseudo-spectral method," *J. Projectiles, Rockets, Missiles Guid.*, vol. 38, no. 6, pp. 95–98, 2018.
[17] J. Yu, X. Dong, Q. Li, and Z. Ren, "Cooperative integrated practical time-varying formation tracking and control for multiple missiles system," *Aerosp. Sci. Technol.*, vol. 93, Oct. 2019, Art. no. 105300.
[18] P. B. Ma and J. Ji, "Three-dimensional multi-missile formation control," *Acta Aeronautica et Astronautica Sinica.*, vol. 31, no. 8, pp. 1660–1666, 2010.
[19] C. Z. Wei, J. Guo, and N. Cui, "Research on the missile formation keeping optimal control for cooperative engagement," *J. Astronaut.*, vol. 31, no. 4, pp. 1043–1050, 2010.
[20] M. X. Peng, Y. J. Wu, and F. T. Zhu, "Research on control method for anti-ship missiles formation flight," *J. Syst. Simul.*, vol. 29, no. 1, pp. 212–217, 2017.
[21] X. Wang, H. Fang, L. Dou, B. Xin, and J. Chen, "Integrated distributed formation flight control with aerodynamic constraints on attitude and control surfaces," *Nonlinear Dyn.*, vol. 91, no. 4, pp. 2331–2345, Mar. 2018.
[22] H. Y. Gao, L. T. Zhou, and Y. L. Cai, "Sliding mode controller design for multi-missiles three-dimension formation flight," in *Proc. 18th CCSSTA*, 2017, pp. 243–246.
[23] L. Zhang, F. Yangwang, and M. Donghui, "Adaptive sliding-mode controller design for missile cooperative engagement," *J. Astronaut.*, vol. 35, no. 6, pp. 700–707, 2014.
[24] X. F. Wang, Y. Y. Zheng, and H. Lin, "Control Method for Missile Formation Flight," *Trans. Beijing Inst. Technol.*, vol. 34, no. 12, pp. 1272–1277, 2014.
[25] L. Zhang, F. Yangwang, D. Xinghua, and H. Jie, "Design of nonlinear optimal controller for multi-missile formation," *J. Beijing Univ. Aeronaut. Astronaut.*, vol. 40, no. 3, pp. 401–406, 2014.
[26] H. B. Zhou, S. M. Song, and Z. Zheng, "Distributed robust adaptive control for missile cooperative engagement within formation," *J. Chin. Inertial Technol.*, vol. 23, no. 4, pp. 516–527, 2015.
[27] S. Mobayen, M. J. Yazdanpanah, and V. J. Majd, "A finite-time tracker for nonholonomic systems using recursive singularity-free FTSM," in *Proc. Amer. Control Conf.*, Jun. 2011, pp. 1720–1725.
[28] S. Mobayen, "Design of LMI-based sliding mode controller with an exponential policy for a class of underactuated systems," *Complexity*, vol. 21, no. 5, pp. 117–124, May 2016.
[29] V. I. Utkin, *Sliding Modes in Control Optimization*. Berlin, Germany: Springer, 1992.
[30] X. Su, X. Liu, P. Shi, and R. Yang, "Sliding mode control of discrete-time switched systems with repeated scalar nonlinearities," *IEEE Trans. Autom. Control*, vol. 62, no. 9, pp. 4604–4610, Sep. 2017.
[31] S. Mobayen and J. Ma, "Robust finite-time composite nonlinear feedback control for synchronization of uncertain chaotic systems with nonlinearity and time-delay," *Chaos, Solitons Fractals*, vol. 114, pp. 46–54, Sep. 2018.
[32] Q. Dong, Q. Zong, B. Tian, C. Zhang, and W. Liu, "Adaptive disturbance observer-based finite-time continuous fault-tolerant control for reentry RLV," *Int. J. Robust Nonlinear Control*, vol. 27, no. 18, pp. 4275–4295, Dec. 2017.
[33] M. You, Q. Zong, B. Tian, X. Zhao, and F. Zeng, "Comprehensive design of uniform robust exact disturbance observer and fixed-time controller for reusable launch vehicles," *IET Control Theory Appl.*, vol. 12, no. 5, pp. 638–648, Mar. 2018.
[34] Y. Meng, B. Jiang, R. Qi, and J. Liu, "Fault-tolerant anti-windup control for hypersonic vehicles in reentry based on ISMDO," *J. Franklin Inst.*, vol. 355, no. 5, pp. 2067–2090, Mar. 2018.
[35] S. Mobayen and F. Tchier, "Nonsingular fast terminal sliding-mode stabilizer for a class of uncertain nonlinear systems based on disturbance observer," *Scientia Iranica*, vol. 24, no. 3, pp. 1410–1418, Jun. 2017.
[36] J. Wang, Y. F. Liu, and Z. Shi, "Three-dimensional guidance law with impact time constraint," *Navigat. Positioning Timing.*, vol. 2, no. 6, pp. 12–18, 2015.
[37] J. Song and S. Song, "Three-dimensional guidance law based on adaptive integral sliding mode control," *Chin. J. Aeronaut.*, vol. 29, no. 1, pp. 202–214, Feb. 2016.
[38] J. P. LaSalle, "Stability theory for ordinary differential equations," *J. Differ. Equ.*, vol. 4, no. 1, pp. 57–65, Jan. 1968.
[39] H.-B. Zhou, S.-M. Song, and J.-H. Song, "Design of sliding mode guidance law with dynamic delay and impact angle constraint," *Int. J. Control, Autom. Syst.*, vol. 15, no. 1, pp. 239–247, Feb. 2017.

ZHENLIN ZHANG received the master's degree in control science and engineering from the School of Astronautics, Northwestern Polytechnical University, Xi'an, China, in 2020, where he is currently pursuing the Ph.D. degree in control science and engineering. His current research interests include multi-missile formation, multi-missile coordination, and reinforcement learning.

KE ZHANG received the Ph.D. degree in chemical engineering from the School of Astronautics, Northwestern Polytechnical University, Xi'an, China, in 1998. He is currently a Professor with the School of Astronautics, Northwestern Polytechnical University. His current research interests include navigation, guidance, and control, image processing, and control theory and control engineering.

ZHIGUO HAN received the Ph.D. degree in chemical engineering from the School of Astronautics, Northwestern Polytechnical University, Xi'an, China, in 2017. He is currently a Teacher with the School of Astronautics, Northwestern Polytechnical University. His current research interests include navigation, guidance and control, multi-missile formation, and multi-missile coordination.